THE ANALYTIC SCIENCES CORPORATION

(NASA-CR-160078) NAVSTAR GLOBAL POSITIONING SYSTEM APPLICABILITY TO THE NATIONAL OCEANIC SATELLITE SYSTEM (Analytic Sciences Corp.) 119 p HC A06/MF A01 CSCL 17G

N81-14990

Unclas
G3/04 29664

TR-3298

NAVSTAR GLOBAL POSITIONING SYSTEM APPLICABILITY TO THE NATIONAL OCEANIC SATELLITE SYSTEM

25 July 1980

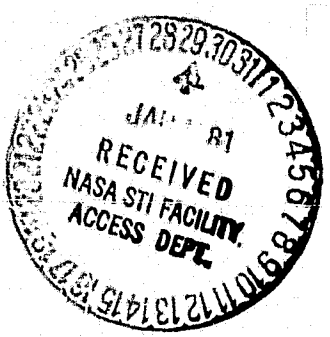

Prepared under

Contract No. NAS 5-26128

for

NATIONAL AERONAUTICS AND SPACE ADMINISTRATION
Goddard Space Flight Center
Greenbelt, Maryland

Prepared by:
G.A. Matchett

Approved by:
H.L. Jones
E.W. Vinje

THE ANALYTIC SCIENCES CORPORATION
Six Jacob Way
Reading, Massachusetts 01867

FOREWORD

The work for this report was performed under contract number NAS 5-26128. The author acknowledges the guidance and assistance of the Contract Technical Monitor, Mr. Mort Friedman of the NOSS Program Office of NASA/Goddard. Assistance and cooperation were also received from Mr. Peter Hui of NASA/Goddard. Ms. Marsha D. O'Connell of TASC played a key role in development of the simulations on which much of the analysis in this report is based.

ABSTRACT

This report presents the results of a preliminary investigation into the potential for applying NAVSTAR Global Positioning System (GPS) user equipment to the spacecraft of the National Oceanic Satellite System (NOSS). Two widely different navigation goals for NOSS spacecraft are examined: one being moderate accuracy, real-time navigation utilizing the simplest of GPS receivers, and the other being precision vertical displacement measurement over limited arcs utilizing specialized GPS equipment, possibly with ground data processing.

A single channel, sequential, single frequency (L1), C/A-code only GPS receiver is concluded to be able to provide moderate accuracy, real-time navigation for NOSS spacecraft. The functional and operational characteristics of such a receiver are examined in comparison with those of similar, current development models. The navigation error sources are examined and are used to simulate the performance of such a receiver, conservatively concluding that positional accuracies of 10 m (1σ) each axis are be expected when 12 or more GPS satellites are in operation. The precision vertical displacement goal of 5 cm over tracking arcs of 500 km or more is concluded to be very near the achievable accuracy limitations with GPS. Further examination and simulation of sophisticated approaches to this problem are warranted.

TABLE OF CONTENTS

LIST OF FIGURES

LIST OF FIGURES (Continued)

LIST OF TABLES

1. INTRODUCTION

This report is on a preliminary study to assess the applicability of the NAVSTAR Global Positioning System (GPS) to the National Oceanic Satellite System (NOSS) in two widely divergent roles. One application is for moderate accuracy, real-time navigation with the simplest of GPS receivers. The other application is as a source for an extreme precision (5 cm) vertical displacement estimator over tracking arcs of 500 km or more, considered without limitations on equipment complexity or data processing methods.

The NOSS program is a joint effort of the Commerce Department, the National Oceanic and Atmospheric Administration, the Defense Department, and the National Aeronautics and Space Administration, with the management activity located at NASA Goddard Space Flight Center. The NOSS spacecraft will carry sensors whose technologies were previously demonstrated on the SEASAT and Nimbus-7 satellites. The first NOSS spacecraft are to be launched in mid 1986 and have design lifetimes of three years.

GPS is a joint service program, managed by the Air Force. It is a satellite-based radio navigation system that will be capable of providing extremely accurate three-dimensional position and velocity information (as well as time and frequency information) to properly equipped, qualified users anywhere on or near the earth. Figure 1-1 is an abbreviated version of a GPS program schedule showing initial operational capability in late 1985 with full capability by the end of 1987. Eighteen satellite vehicles will form the full Phase III operational constellation. There are currently six satellite vehicles

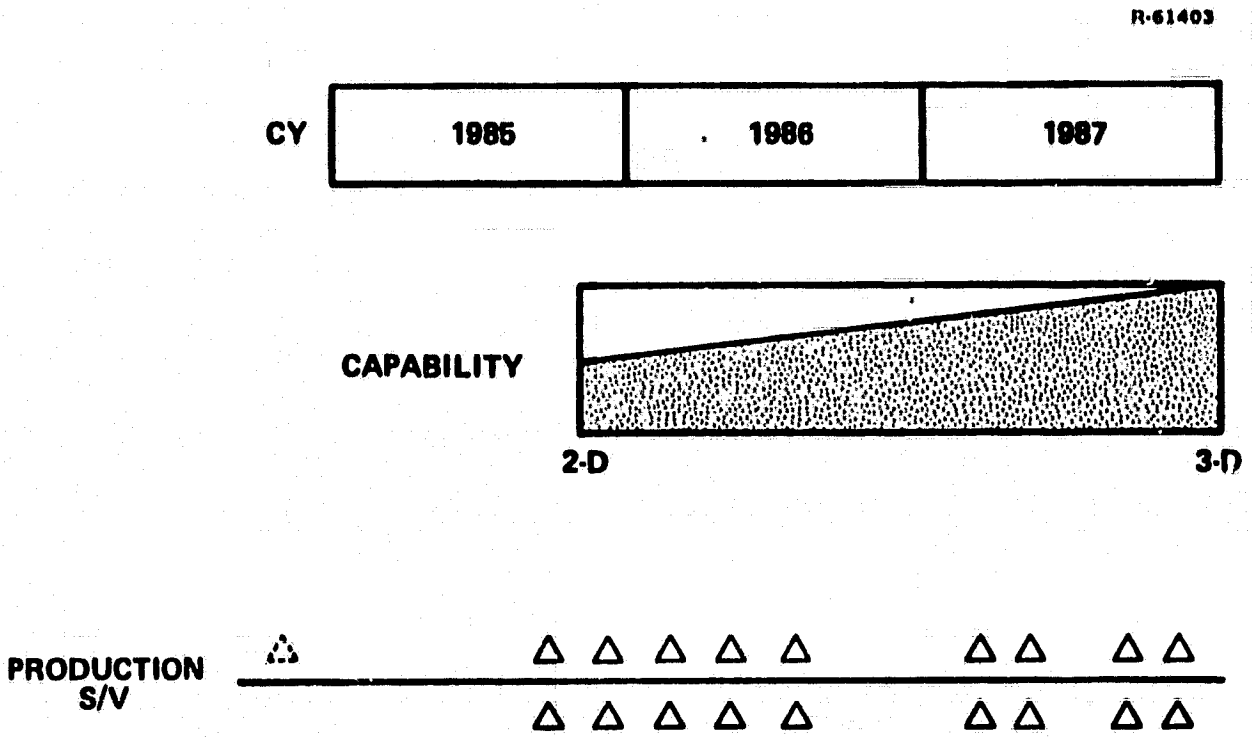

Figure 1-1 Current GPS Program Schedule

orbiting in a Phase II test constellation. One of these is no longer operational, and one was only recently launched. The other four have been tested extensively and, except for clock reliability problems, are generally performing beyond expectations.

The remainder of this chapter is an introduction to GPS operating principles useful in understanding the material to follow (Refs. 1 to 8). Chapter 2 is a summary of the recommendations for parameters of the GPS user equipment that will meet the moderate accuracy navigation requirement for NOSS. Along with those recommended values are comparisons to four developmental model GPS receivers that most closely resemble the recommended design. Chapter 3 is a short survey of the sources of GPS navigation error relevant to the moderate accuracy NOSS requirement, with a detailed development of ionospheric delay errors left to Appendix A. Chapter 4 (still

addressing the moderate accuracy requirement) considers navigation accuracy and has three major sections: one on GPS satellite visibility, one on the design of a navigation filter algorithm suitable for the NOSS GPS receiver, and one on simulation results of an error covariance analysis of two NOSS navigation scenarios. Navigation filter design details and evaluation methods are more fully discussed in Appendix B. Chapter 5 is devoted to the precision vertical displacement estimation problem. Chapter 6 is a short summary of the most important conclusions and recommendations of this study.

1.1 GPS OPERATING PRINCIPLES

Each GPS satellite broadcasts a navigation signal with three components. These components consist of both a clear/acquisition (C/A) signal and a precision (P) signal centered about the Link 1 L-band carrier frequency, and either the C/A or the P signal centered about the Link 2 L-band carrier frequency. The carrier frequencies are integral multiples of the basic satellite clock frequency of 10.23 MHz:

$$L1 = 1575.42 \text{ MHz} = 154 \times 10.23 \text{ MHz}$$

$$L2 = 1227.60 \text{ MHz} = 120 \times 10.23 \text{ MHz}$$

The C/A or the P signal is generated by using a standardized, high rate, pseudo random noise (PN) binary sequence (termed the C/A-code or the P-code), summed modulo 2 with a low rate (50 Hz) binary navigation data message to bi-phase shift key modulate the carrier frequency (Fig. 1.1-1). The C/A signal and the P signal are in phase quadrature on L1. The result is spread spectrum signals with bandwidths of approximately 20 MHz. Each satellite uses a C/A-code and P-code different from that used by any other satellite so that the signals may be

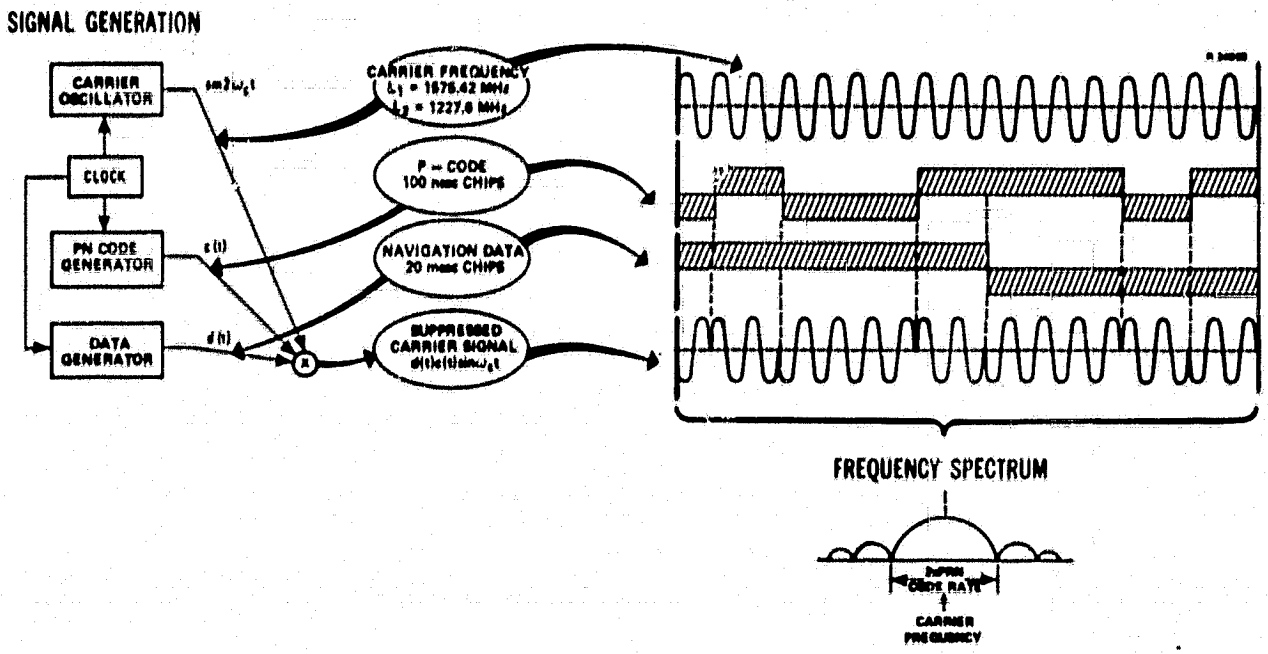

Figure 1.1-1 GPS Signal Structure (P-Code only)

distinguished, as all the satellites use the same carrier frequencies.

The chipping rate of the P-code is the basic clock frequency of 10.23 MHz, corresponding to a chip width of 100 nsec, and the effective length of the P-code is one week,* or about 6×10^{12} chips. The way in which the signals are detected is to generate a replica code within the receiver and attempt to correlate it to the code of the incoming signal. No information is obtained from this process unless the replica code is synchronized within one-half chip of the incoming code. The high chipping rate and long effective length of the P-code make direct signal acquisition impractical unless the user

*In fact, there is only one P-code, and that is 37 weeks long. Each satellite uses a different one week segment of this code and reinitializes it once per week.

receiver already has a very good estimate of where to start looking, and that implies a very good estimate of time and of user distance from the GPS satellite. This information is generally unavailable in first acquiring a satellite signal, and it is for this reason that the C/A signal is supplied. The chipping rate of the C/A-code is only 1.023 MHz, and, more importantly, the length of the C/A-code is only 1 ms (1023 chips). In attempting to match a replica C/A-code to that of the incoming signal only 2046 trials must be made to ensure being synchronized within one-half chip.* Once the C/A signal is detected, the low rate navigation data message superimposed on it may be interpreted. Every six seconds in this message is a "handover" word that may be used† to synchronize the P-code.

The replica code used for detecting the signal is generated by a clock that is part of the user receiver. If the receiver clock were synchronized to GPS system time, then the replica code would have to be delayed by the signal propagation time (from GPS satellite to the user receiver) in order to match the code of the incoming signal. An additional advance or delay of the replica code would be necessary to account for an offset of the user clock with respect to GPS system time. It is the total amount by which the replica code is delayed when synchronization is achieved that is the basic navigation measurement, termed pseudo range. If the signal were propagated at the constant speed of light in vacuum, then pseudo range would be a measure of the actual range from the user to the GPS satellite, plus the offset in the user clock phase. Since navigation concerns itself with positions and ranges, in the ensuing analyses clock phase offsets and time delays will often be

*This situation may be complicated by user dynamics.

†Only certain, qualified users may be permitted access to the P-code; special hardware may be required.

measured in units of distance, converted by using the speed of light (3×10^8 mps, unless more accuracy is warranted).

GPS receivers actually estimate both code phase and carrier phase while tracking a signal in their most accurate mode. By differencing beginning and ending pseudo range measurements made over a period when carrier phase lock is achieved, an "integrated doppler" measurement of "delta range" is made. When the doppler processing period is short and the delta range measurement is divided by the period, the measurement is termed pseudo range-rate. Pseudo range-rate is the time derivative of pseudo range and is a measure of the rate at which the range from the user to the GPS satellite is changing, plus the frequency offset of the user clock. Just as clock phase offsets or time periods are measurable in units of distance, so frequency offsets are measureable in units of velocity, by multiplying by the speed of light.

Measurements of pseudo range and of pseudo range-rate, along with the navigation data extracted from the signals, are used in a computer portion of the user receiver to solve for user position, velocity, clock phase, and clock frequency. Before discussing the navigation algorithm that performs this task, some further consideration should be given to the measurements themselves and to the navigation data message.

A receiver can typically match the replica code with the incoming code to a small fraction of a chip; the quantization level is 1/64 of a chip in some designs, although this does not imply the overall accuracy level. A C/A-code chip is about 293 m long, while a P-code chip is one-tenth as large. Even though the C/A signal is provided primarily for acquisition purposes, users with moderate navigation accuracy needs may opt to use it alone, saving the cost (and "qualification" problems) of using the P-code.

The dual frequency (L1 and L2) operation is provided because the signals are additionally delayed in passing through the ionosphere by an amount inversely proportional to frequency squared. Measurements at two frequencies may be used to compensate for the ionospheric delay. Such compensation is useful primarily to those needing P-code type accuracy. In fact, currently only the P-code is available on L2, a situation likely to continue.* A receiver designed for C/A-code only would almost surely be for L1 frequency only, an additional simplification.

Because each pseudo range measurement is a mixture of four unknown quantities -- three components of user position and the user clock phase offset -- many users need to make four simultaneous measurements of pseudo range to four different satellites and then solve directly for user position and time. That implies four receiver channels operating at once. Some users are able to estimate position by a more indirect approach, often by taking advantage of independent knowledge of their dynamics, and are able to process sequentially-generated measurements. Such users could opt for a single channel (or dual channel) receiver.

A discussion of single versus multiple channel receivers is an appropriate place to raise the issue of intentional or unintentional interference with the GPS signals. Radio Frequency Interference (RFI), or "jamming" if it is intentional, is raised as an issue partly because it might be of some direct interest to the designers of NOSS, and partly because it has had a strong impact on GPS system design and on the ways in which other users approach the system. The process of correlating the receiver-generated replica code to the code

*There have been requests to put C/A-code on L2, but probably only for limited test purposes.

of the incoming signal narrows the spectrum of the GPS signals while it spreads the spectrum of continuous wave, swept continuous wave, or narrow band interfering noise. The narrow, closed-loop bandwidths of the tracking loops then reject most of the noise, reducing the effective interference level by the processing gain for the code (70 dB-Hz for P-code, 60 dB-Hz for C/A-Code). In open-loop acquisition of these codes, before correlation is achieved, the resistance to interference is about 20 dB lower. Users with high dynamical uncertainties operating in a high interference environment thus have an additional reason to opt for a multichannel receiver: so they can avoid the reacquisition process. Users with low dynamical uncertainties can perform a closed-loop reacquisition, without increasing their susceptability to interference.

The 50 Hz navigation data message superimposed on the GPS signals is formatted in 30 sec (1500 bit) frames, which are subdivided into five 6 sec (300 bit) subframes (Fig. 1.1-2).

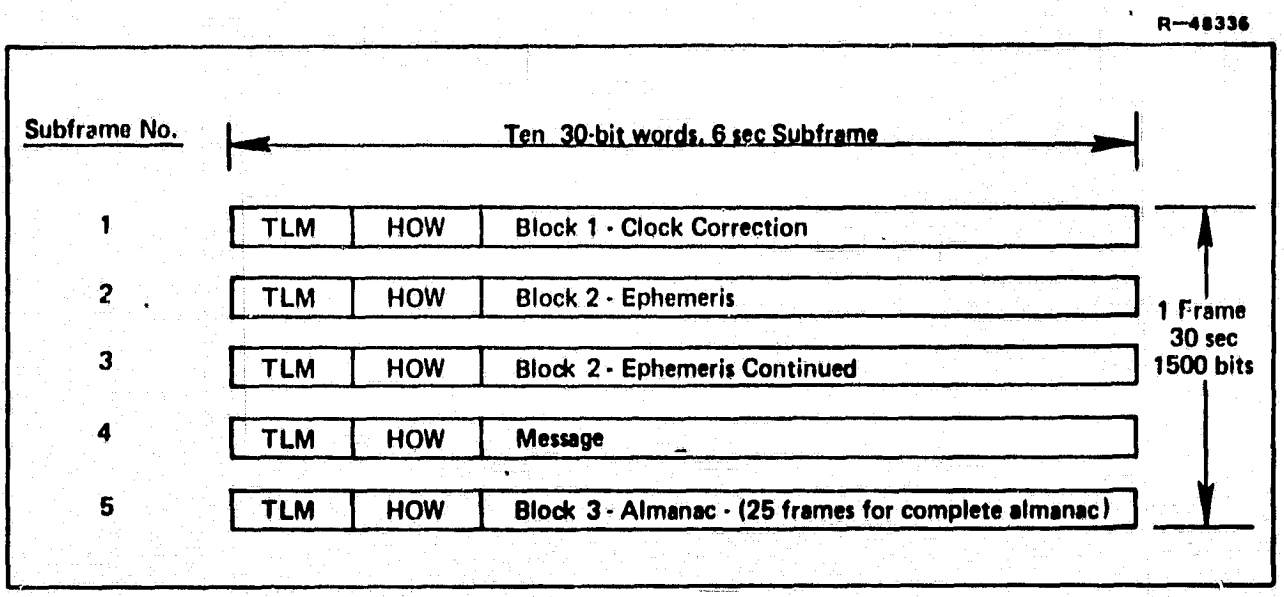

Figure 1.1-2 GPS Navigation Data Format -- Frame and Subframe Structure

Each frame contains several different types of data. It has already been noted that a handover word (HOW) to help in acquiring the P signal is repeated every six seconds (every subframe) in this message. Preceeding the handover word is a telemetry word (TLM) containing a synchronization pattern (so it may be recognized) and various health and status indicators indicating whether the signal is usable or not. The handover word itself is nothing more than a precise measure of the time since the beginning of the week.

The remainder of the navigation message consists of three data blocks (and an alphanumeric message block reserved for unspecified future use). Data Block 1 appears every 30 seconds and contains the GPS satellite clock correction coefficients and ionospheric delay model coefficients for single frequency users.* It is necessary to interpret Data Block 1 to adjust the measurements for GPS satellite clock errors before using the measurements in the navigation solution. Data Block 2 contains coefficients that allow the GPS satellite position and velocity to be computed as functions of time using a specified model in the user receiver computer. This precision ephemeris data is also repeated every 30 seconds and also must be interpreted to allow the measurements to be used in the navigation solution.

The precision ephemeris and clock coefficients are revised by the GPS satellite once per hour, but are useful for a period of 90 min from their first appearance. Even after 90 min, the quality of the ephemeris and clock corrections based on "old" coefficients degrades gracefully. A near-earth orbital user of GPS, such as the NOSS spacecraft, will typically see a GPS satellite for some segment of an orbit (15 to 45 min)

*This model is not yet specified and may not be suitable for space-based users.

and then not see that satellite again until the following orbit, about 90 min after the first appearance. In this case, Data Blocks 1 and 2 need to be interpreted on the first appearance of each GPS satellite on each orbit: With a single channel receiver, the channel will likely be devoted to one satellite for the 30 sec it may take to gather this data.

Data Block 3 contains what is known as Almanac data. The Almanacs contain ephemeris representation parameters, clock correction parameters, and health and status indicators. This data is a truncated, less accurate version of the data in Blocks 1 and 2. It is useful in initial acquisition of satellite signals. The precision data in Blocks 1 and 2 pertains only to that GPS satellite that broadcasts it, but each satellite broadcasts Almanac data for the entire constellation of satellites. The Almanac data contains one "page" (pertaining to one GPS satellite) every 30 sec. When 24 satellites were planned for the operational constellation, 25 pages were assigned to Almanac data, meaning that it would take 750 sec (12.5 min) to gather the entire Almanac. Now that only 18 satellites are planned for the operational constellation, the Almanac data presentation may change too.

Almanac data, being of lesser precision, is only renewed every six days and is usable to support C/A signal acquisition for five weeks or more. A receiver in a continuous mode of operation need never renew its Almanac data unless GPS satellite signals change character (as for example, a new satellite were to join the constellation or a satellite were to switch internal clocks on ground command). In any event, the Almanac data can be pieced together a page at a time while the precision navigation data is being collected. The only impact of the Almanac for a GPS receiver on a NOSS spacecraft would

be that either some data link must be established to initialize the Almanac, or a long (20 min) initialization period must be assumed after the set is first turned on before it generates useful navigation output. If it is desired to cold start the set after ejection of the NOSS spacecraft from the Shuttle and then use the navigation outputs immediately to help establish a transfer orbit, a data link or some nonvolatile memory for the Almanac would be needed.

The final topic to be discussed under this general heading of operating principles is the navigation algorithm that resides in the receiver computer and turns GPS measurements into navigation outputs. As was mentioned, one method uses four simultaneous measurements to four different GPS satellites and solves deterministically for user position and clock offset. This is a straightforward matter of solving four simultaneous nonlinear equations in four unknowns. Much of the accuracy literature on GPS usage assumes this type of navigation algorithm. If the errors in the four simultaneous pseudo range measurements are independent from one another and if they are of equal variance, then the navigation errors resulting from the deterministic solution are related to the pseudo range errors by factors known as geometric dilution of precision (GDOP) factors. Usually, the term GDOP is reserved for the four-dimensional root-sum-square (rss) combination of position and time errors, with other terms (VDOP, HDOP, PDOP) being used when vertical, horizontal, or three-axis position errors are considered. Under the assumptions above, the standard deviation of the resultant navigation error is equal to the appropriate dilution of precision factor times the standard deviation of a single pseudo range error.

Another type of navigation algorithm is available to a user who

- has excellent knowledge of his dynamics (for example an earth-fixed user or a nonthrusting spacecraft user),
- wishes to integrate other navigation data with GPS data in the navigation solution (a user with an inertial navigation system, other radio aids, an altimeter, etc.), or
- has relatively low level dynamics and wishes to use a single channel receiver.

The latter is the likely case for NOSS spacecraft application. The navigation algorithm appropriate to this case is some version of a Kalman filter which sequentially processes single GPS measurements as they are obtained. Designing such a filter requires detailed knowledge of the special considerations that led to its selection, especially of the user vehicle dynamics.

An adjunct to the navigation algorithm are two other computational capabilities associated with the receiver. One is a satellite selection algorithm that decides which satellites to use in making GPS measurements. Tradeoffs are made among measurement accuracy, measurement geometry, acquisition time, navigation data availability, and satellite visibility. The other capability is specialized to the user application and consists of transforming the navigational output into more usable form. Generally, the navigation outputs are in the form of latitude, longitude, and altitude with respect to the World Geodetic System 1972 (WGS'72) ellipsoid, but most users wish auxiliary outputs in coordinates of their own choosing.

2. GPS USER EQUIPMENT

This chapter contains a partial description of the functional and operational characteristics of GPS user equipment appropriate to the moderate accuracy navigation requirement for NOSS. It also contains a discussion of several development model GPS receivers most comparable to the recommended design, including one receiver (GPSPAC) designed for a similar spacecraft environment.

There is a long list of requirements that need consideration in specifying GPS user equipment suitable for the moderate accuracy navigation requirement for NOSS spacecraft application. Heading this list are the overall functional requirements of size, weight, power, MTBF, navigation accuracy, and cost. Before these may be considered, it is necessary to examine the more detailed functional requirements such as the number of receiver channels, the operating frequencies, the GPS codes, the receiver computer, the receiver operating modes, and the command/data interfaces. Interlaced with the functional requirements are the operational requirements in terms of required signal power, signal dynamical ranges, measurement frequency, measurement accuracy, stabilization time, and time-to-first-fix (TTFF). Finally, consideration must be given to environmental requirements, such as temperature ranges, pressure altitude limits, g-loading, vibration, shock, radiation, and the like, from both operability and survivability standpoints.

The major focus of this report is on navigation accuracy and its relationship to the detailed functional and operational requirements of the GPS user equipment. Accuracy is

investigated in detail in Chapters 3 and 4, and the results of that investigation will be assumed here. Environmental considerations will be deferred to the spacecraft designers, as such requirements typically do not impact the accuracy issue.

Recommendations for GPS user equipment parameters are presented along with results of a survey of current, (Phase I) developmental GPS receivers that are most similar to that appropriate to the NOSS application. Four receivers were selected for comparison purposes. Three of them are related; the Z set, the Manpack, and the GPSPAC are all under development by Magnavox. The names Z set and Manpack are generic; they were defined by the GPS Joint Program Office (JPO) (Ref. 9) and are under development by more than one manufacturer. The versions reported on here under these names are strictly those by Magnavox. The GPSPAC is a derivative of the Manpack intended for use aboard a satellite (originally SEASAT, then LANDSAT D as schedules changed) very much similar to the NOSS spacecraft in environment. The fourth receiver considered is termed the Manpack/Vehicular User Equipment (MVUE) and is under development by Texas Instruments. The Phase II family of modular GPS user equipment is currently under development by Magnavox and Collins Radio. Performance characteristics for those receivers are not yet available.

Figures 2-1 and 2-2 are block diagrams for the Z set and GPSPAC. They show the modular design of the receivers and the relationship of the receivers to their environment. The Z set, being a single frequency set, has a bandpass filter (BPF) and preamplifier at the antenna, and is connected to a control/display unit. The two tracking loops of the single receiver channel are illustrated. The process controller and the data processor blocks are both part of the computer modules within the receiver, and they reflect the dual function of this unit.

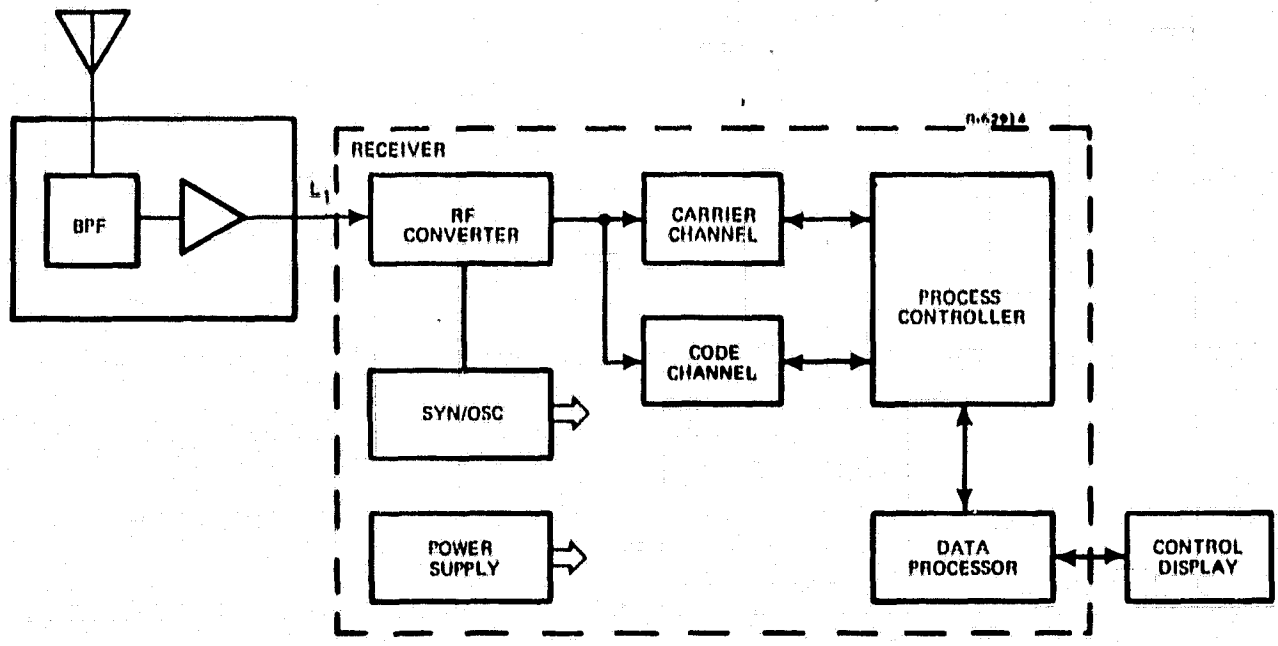

Figure 2-1 User Equipment Set Z Block Diagram (Ref. 10)

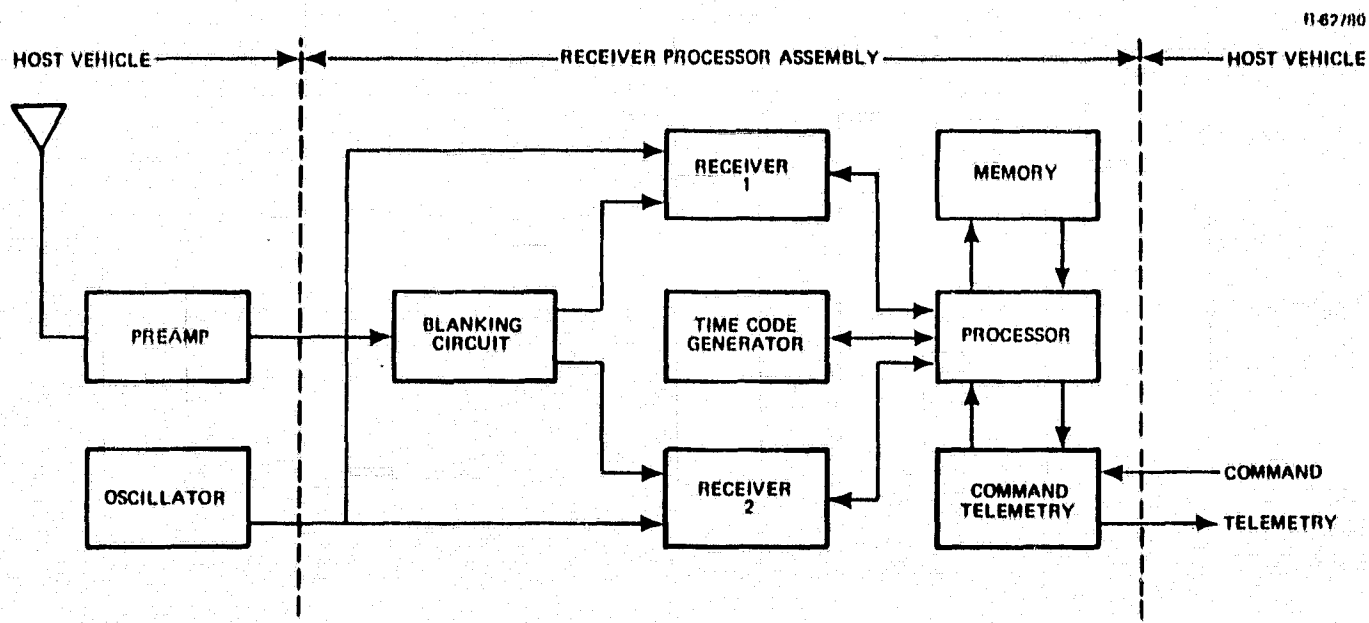

Figure 2-2 GPSPAC Block Diagram (Ref. 11)

The synchronization/oscillator block is often referred to as the user clock. The GPSPAC, in contrast to the Z set, has provision for an external oscillator as well as for an internal one. Being a two frequency set, it has a wideband preamp without a bandpass filter. The blanking circuit is to protect the RF stages from overload when spacecraft transmitters are active. Two complete receiver channels are shown, as is a command and telemetry interface module.

It might seem surprising that two of the sets chosen for investigation are designed to be man-carried, while the application under discussion is in an orbiting satellite. In fact, the applications are strongly related by the user dynamical uncertainty level. A spacecraft in orbit experiences very low disturbing forces and its dynamics are very highly predictable. A man-carried receiver, placed on the ground, has a somewhat similar dynamical predictability. Both applications can utilize a simple, single channel, sequential receiver unlike that required by more dynamic users. There are other similiarities. A man can shield a hand carried receiver against intentional jamming by simply blocking part of the antenna coverage zone. Intentional jamming of a satellite-borne, upward-looking receiver is difficult and unlikely. Manpack receivers run on batteries and are more power conscious than are vehicular sets, a consciousness likely to be shared by satellite-borne equipment for extended missions.

Besides the obvious environmental differences, there are two functional/operational differences between suitable parameters for a Manpack and for a spacecraft-borne receiver. One difference is in signal dymanics, where the spacecraft receiver must work at much higher relative velocity levels (relative to the GPS satellites) but at much lower relative

jerk levels than does the Manpack. This difference is easily accommodated in hardware design. The other difference is in required reliability. The intermittently used and serviceable Manpack needs far less reliability than does the continuously used, long mission, spacecraft set. This difference is not easily accommodated in hardware design; the spacecraft needs are difficult to meet at any cost and may require redundancy at a high level.

Table 2-1 summarizes the recommended parameters for a receiver suited to the NOSS application and compares them with the values for the Phase I receivers. Some of the material in the table is two and three years old, and may not precisely reflect current design values. A good place to begin to discuss the table is after the first group of overall functional parameters, coming back to these later.

As the results of Chapters 3 and 4 show, a single channel, single frequency, single code receiver will be adequate for NOSS application. All of the sets considered have only one channel, except for GPSPAC, and it has two channels for redundancy and to examine the need for simultaneous two frequency operation to compensate ionospheric errors. The Manpacks and derivative sets have two frequency, P-code capability primarily to handle the ionospheric error problem. That problem can be partly solved for NOSS by restricting antenna viewing angles to upward looking signal paths from orbital altitudes above most of the ionospheric electrons.

The memory size shown is quite variable, depending on the architecture of the receiver. The computer portion of the receiver is intimately tied to the signal tracking loops and a major portion of its time and memory are devoted to running the loops. A minor portion is devoted to the navigation and

TABLE 2-1
COMPARISON OF RECEIVER SPECIFICATIONS

T-4322

PARAMETER	UNITS	RECEIVER TYPE				
		NOSS	Z SET	MANPACK	GPSPAC	MVUE
Size	kcc	4-16	17	12	26	23
Weight	kg	5-11	12	11	17	15
Power	W	10-25	50	26	25	45
MTBF	khr	50	1/2	1/2	20	2
Accuracy (per position axis)	m(1σ)	10	10[1]	3[1]	3[1]	3[1]
Cost	$K	?	15-25	16-22	85-?	15
Number of Channels	#	1	1	1	2	1
Frequencies	L1, L2	L1	L1	L1 and L2	L1 and L2	L1 and L2
Codes	C/A, P	C/A	C/A	C/A and P	C/A and P	C/A and P
Memory Size (16 bit words)	K	40	NA[2]	NA[2]	40	48
Antenna Coverage (half-cone angle)	deg	85	85	80	100	NA[2]
Signal Power, High	dBW	-150	-130	-150	-151	-156
Low	dBW	-165	-163	-163	-167	-166
Signal Dynamics, Range	Mm	18-27	NA[2]	NA[2]	18-27	NA[2]
Range-Rate	km/s	±9	±4.5	±4.5	±9	±4.5
Range Acceleration	m/s^2	±16	±30	±20	±16	±16
Range Jerk	mm/s^3	±20	±50000	±4000	±20	NA
Measurement Frequency	#/min	1-5	4-6	4-6	8-12	30
Measurement Accuracy, Range	m(1σ)	15	15	1.5 (P)	1.5 (P)	1.6 (P)
Range-Rate	mm/s(1σ)	8-25	24	24	NA[2]	NA[2]
Stabilization Time	min	5	5	3	5	4
Time-To-First-Fix	min	5	5	15	NA[2]	NA[2]
Data Reference			Ref. 10	Ref. 10	Ref. 11	Ref. 7

NOTES:

1. Rough accuracy estimate for NOSS spacecraft environment; does not agree with published values for other environments.
2. Information not available.

peripheral calculations. Future receiver designs may simply beat the incoming signal against a carrier frequency oscillator, bandpass filter, sample the results, and perform the rest of the signal processing totally digitally. This is especially true of C/A-only sets, since C/A-codes have a bandwidth of only 1 MHz. All-digital design would, of course, depend more heavily on the computer, but it might well lead to overall simplification and reliability enhancement.

Antenna coverage is deliberately restricted for NOSS to counter ionospheric delay errors discussed in Chapter 3 and Appendix A. The value of 85 deg refers to an antenna pointed at the zenith covering a region down to 85 deg from the zenith (5 deg above the horizontal). Signal power is not much of an issue, especially when ionospheric and tropospheric losses may be ignored, and when antenna viewing limits serve to limit the range to a GPS satellite. The minimum value recommended could probably be raised if any significant tradeoff advantage could be found. Signal dynamics refer to the geometric range between the user and a GPS satellite. The recommended values can comfortably accommodate the range to be expected from a NOSS spacecraft, even though the GPS satellite orbital details are not all firm.

The measurement frequency needed to navigate a non-thrusting spacecraft is very low, even lower than the values shown. Measurement accuracy values are typical for C/A-code ranging. For range-rate measurements, the receiver may be designed to take advantage of the benign spacecraft environment by tightening the carrier loop bandwidths and lengthening the delta range processing time, thus improving measurement quality. This has <u>not</u> been assumed in the accuracy investigation, but sensitivity relationships have been provided to assess the impact of improving range rate measurement accuracy.

Receiver stabilization time and time-to-first-fix (TTFF) are only important for the NOSS application if it is desired to use the GPS receiver to assist in establishing a transfer orbit for the spacecraft during the launch to orbit sequence. Depending on the oscillator type chosen and on its stabilization characteristics, the values recommended may be achievable.

The overall functional parameter recommendations for size, weight, and power were assembled by looking at what is being achieved and (for the lower values) by looking into the future (Ref. 10). The lower values are predicted for the 1985 time frame and assume an all-digital system with extensive hybrid/LSI. The 50000 hr MTBF comes from the three year (26000 hr) design lifetime of the NOSS spacecraft, and is likely to be a strong cost driver.

The cost figures need special consideration. They are, for the Z set, the Manpack, and the MVUE, projections in 1977 dollars for thousands of units yet unbuilt. For GPSPAC, the original quote is listed, although the actual cost has escalated well beyond that figure. Most of the cost growth for GPSPAC may be ascribed to development delays in the Manpack program, to which the GPSPAC program was intimately tied. The space qualification and reliability goals also impact GPSPAC cost.

Tables 2-2 and 2-3 show size, weight, power, and cost breakdown in percentage terms for the various modules of the Z set and the Manpack (Ref. 10). These may be useful in gaining a "feel" for the overall features of the receiver hardware. They show the great importance of the computer function within the receiver.

TABLE 2-2

Z SET SIZE, WEIGHT, POWER, AND COST BREAKDOWN

MODULE	PERCENTAGES BY MODULE			
	SIZE (16600 cc)	WEIGHT (12 kg)	POWER (50 W)	COST (see text)
Process Controller/ Data Processor	32	19	60	25
Chassis	-	39	-	6
RF Converter	11	7	10	20
Code Channel	17	4	8	16
Carrier Channel	17	7	10	18
Synthesizer	6	7	10	5
Oscillator	6	2	2	2
Power Supply	11	15	-	8

TABLE 2-3

MANPACK SET SIZE, WEIGHT, POWER, AND COST BREAKDOWN

MODULE	PERCENTAGES BY MODULE			
	SIZE (11960 cc)	WEIGHT (11 Kg)	POWER (26 W)	COST (see text)
Process Controller/ Data Processor	37	13	27	33
Chassis	-	45	-	23
RF Converter	10	5	13	4
Code Channel	7	4	19	13
Carrier Channel	17	4	29	21
Synthesizer	4	3	8	3
Oscillator	3	1	4	2
Power Supply	22	25	-	1

One facet of receiver design not included in the table is that of operating modes. At least three modes will be required for the NOSS application: off, command/telemetry, and navigate. The off and navigate modes are obvious. The command/telemetry mode is less obvious. Some method must be used to initialize the set, and the most efficient is probably to telemeter at least some part of, if not all of, an initial program and data load. The GPS Almanacs and some rough initial spacecraft position and velocity would speed startup. The ability to command the set to telemeter various internal operating values back to earth will be very useful for analysis should anything go wrong, and the ability to command program and data changes will allow some problems to be corrected or bypassed.

The issue of "selective availability" may demand some command link to the set. The basic GPS C/A-code accuracy will probably be deliberately made much worse than that assumed in the remainder of this report. Recovery from this deliberate reduction in system accuracy via software modification (for C/A-code) will be available to qualified users -- if they have a secure command link to the set.

Another use of a command link mode is to instruct the set to favor or to not use specific GPS satellites for navigation. Ground information on GPS satellite health and status may lead to conclusions that would not be reached by onboard software examining the health and status bits of the navigation message. Changing ionospheric model parameters could be uploaded to the receiver should those included in the GPS navigation data be unsuited to spacecraft use. Changing atmospheric density profiles for use by the receiver navigation filter in predicting air drag could also be uplinked.

Further modes, such as calibration, standby, or Almanac data collection, may be desirable. With only one channel, one code, and one frequency, there are few options for navigation modes; one will probably suffice for use on orbit, others may be required for ground checkout.

3. NAVIGATION ERROR SOURCES

Sources of error in navigating with GPS may be categorized into three major segments: the GPS satellite segment, the signal propagation link, and the user segment. As far as the user is concerned, the GPS satellite segment may contribute two types of error, one being an error in the satellite ephemeris data broadcast as part of the navigation message, and the other being an error in the satellite clock correction data contained in the same message. Generally, three types of errors are considered in the propagation link: ionospheric signal delay, tropospheric signal delay, and multipath effects. Considering the NOSS spacecraft as the potential user should eliminate consideration of tropospheric errors and, with some slight consideration given to antenna mounting on the spacecraft, also eliminate consideration of multipath effects. There are two types of error associated with the user segment: signal tracking errors in making GPS measurements, and mechanization errors in turning GPS measurements into navigation outputs. The principal navigation error sources and their expected magnitudes in the NOSS environment are discussed in this chapter.

The errors in the GPS satellite ephemeris and clock correction parameters broadcast by the satellites as part of the navigation message were not modeled in the NOSS performance analysis because these errors are not dominant for moderate accuracy, C/A signal navigation. Proper consideration of the satellite errors involves the satellite orbital dynamics, the satellite clock behavior, the ground tracking network, its clocks, and its measurement errors, and the effects of orbital

prediction. A GPS uploading station (probably colocated with the master control station) will upload to each satellite once per day (at the time of closest approach) the information necessary to prepare the broadcast navigation messages. To some extent, errors in the satellite ephemeris and clock parameters depend on the time since last uploading. Detailed models of the GPS satellite segment errors are to be found in Refs. 12, 13, and 14. Figures 3-1 and 3-2 (Ref. 12) show the results of a detailed covariance analysis of GPS satellite segment errors. They plot the typical contribution to user measurement errors of the satellite ephemeris and clock errors.

Propagation link errors are essentially ionospheric signal delay errors for the NOSS spacecraft application, as tropospheric and multipath errors need not be considered. Appendix A treats the ionospheric ranging errors in some detail, showing that errors for a NOSS spacecraft user could be as high as 90 m. Such high errors would completely dominate the navigation error budget. Fortunately, they may be largely avoided.

In the first place, the error plots of the appendix apply to a worst case situation: daytime at a sunspot cycle maximum. Generally, errors will be from a factor of two to an order of magnitude or more smaller. Given the long projected mission of the NOSS spacecraft, however, the worst case must be considered. Secondly, the ionospheric errors are strong functions of the zenith angle of the signal path, as is shown in the appendix. Looking upwards toward the zenith avoids the regions of peak ionospheric electron density and produces small errors. Looking tangentially downwards through the ionospheric shell produces the peak effects. Limiting the user antenna or the satellite selection algorithm to GPS satellites less than 85 deg from the zenith reduces the worst case errors to less

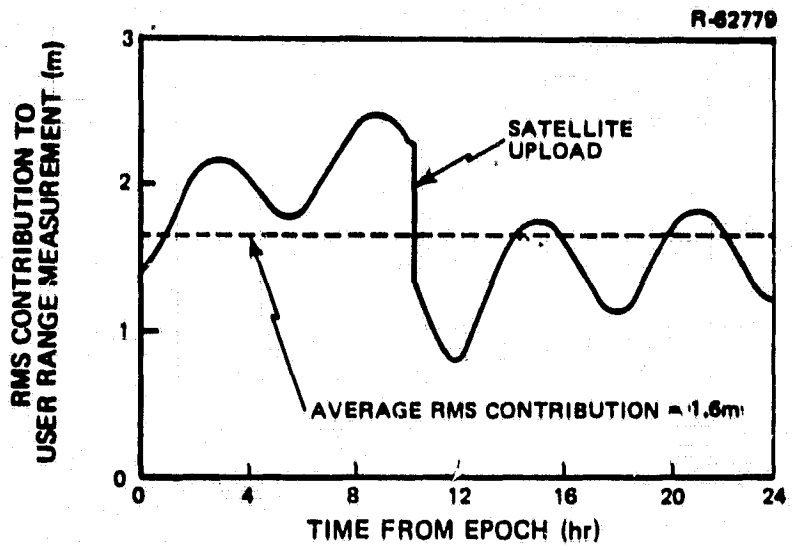

Figure 3-1 Typical RMS Contribution of Uploaded GPS Satellite Errors to User Range Measurement

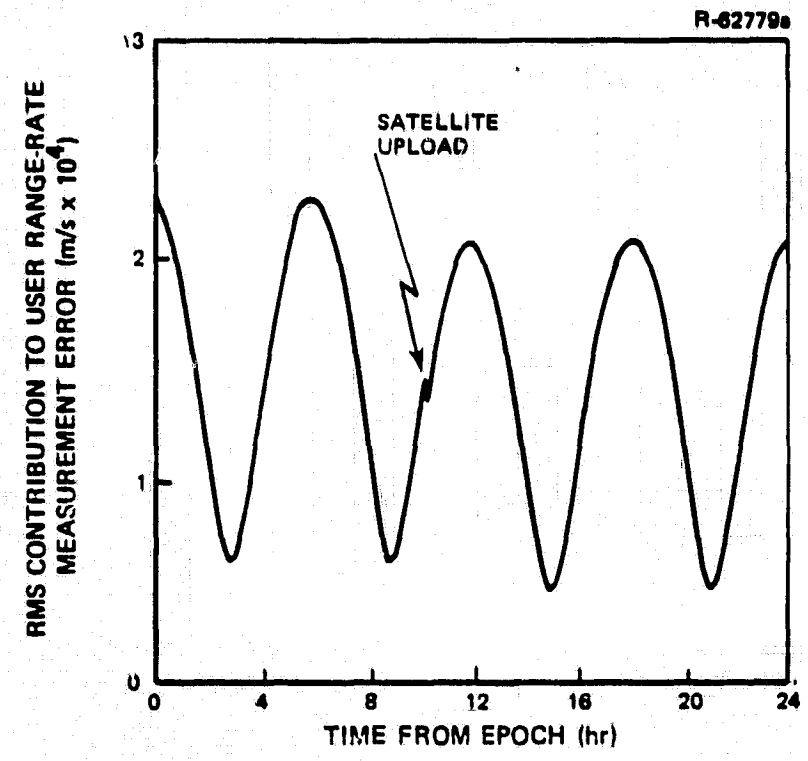

Figure 3-2 Typical RMS Contribution of Uploaded GPS Satellite Errors to User Range-Rate Measurement

than 12 m. For more typical zenith angles, say 60 deg, the worst case errors are less than 6 m. Thirdly, ionospheric modeling in the receiver computer could be utilized to compensate for some of the ionospheric delay. A conservative estimate would be a 50% reduction in ionospheric errors with modeling, putting worst case errors in the range of 3 to 6 m and more typical errors at 1 to 2 m.

Ionospheric delay errors may also affect delta range or pseudo range-rate measurements if the ionospheric delay changes during the doppler processing interval. The delay may change either because the ionosphere is changing or because the signal path through the ionosphere is changing due to movement of the user or of the GPS satellites. These errors are typically very small, from a worst case of about 0.007 mps to a more typical 0.0003 mps or less.

The final source of measurement errors is the user equipment itself. Models of the receiver measurement noise depend to some extent on the design of the signal tracking loops. The parameters in the models are the code loop and (sometimes) the IF bandwidths (the smaller the bandwidths the less the errors) and the signal-to-noise-density ratios (the higher the signal-to-noise-density the less the errors). All else being equal, the pseudo range measurement error is proportional to the code chip width. References 16 to 22 model the receiver measurement errors in considerable detail for a number of mechanizations, especially in the presence of intentional jamming.

No intentional jamming is anticipated for the NOSS spacecraft application, so the signal-to-noise-density is dominated by thermal noise. A 150 Hz figure for IF bandwidth is typical (this bandwidth must pass the 50 Hz navigation data

message) while the code loop bandwidth may easily be kept to 1 Hz. These values lead to a C/A-code pseudo range measurement noise value of about 10 m rms.

When making delta range measurements, the mean square receiver error is proportional to the ratio of carrier tracking loop bandwidth (typically about 20 Hz) to the signal-to-noise-density, and to carrier wavelength squared. Typical values (conservative for the NOSS application) are about 0.6 cm at the L1 frequency. Note that this error is not dependent on which signal (C/A or P) is being tracked, except that the effective signal-to-noise-density ratio for the P signal will be better than that for the C/A signal if intentional jamming is present. To be expressed in terms of pseudo range-rate errors, the delta range measurement error must be divided by the doppler processing interval. This value is typically 0.1 to 0.5 sec, but for the NOSS application it could be made significantly longer (while reducing the carrier loop bandwidth) -- up to several seconds. At a conservative level of 0.25 sec tracking time, the receiver pseudo range-rate error will be about 0.024 mps.

The preceeding discussion covers the sources of the measurement errors, but that does not complete the error discussion. There remain the mechanization errors in the receiver in turning the measurements into navigation outputs. As was previously mentioned, there are two generic ways to mechanize the navigation solution. One way is deterministic, and the relationship between the navigation errors and the measurement errors is best described by geometric dilution of precision (GDOP) factors in this case. The other way, the way suited to the NOSS spacecraft application, utilizes an extended Kalman (or Kalman-like) filter to estimate the navigation state of the vehicle. Chapter 4 of this report contains an analysis and simulation of the navigation errors likely to result from

the use of such a filter in the NOSS application. The error inputs to that simulation are conservatively derived from the values discussed in this chapter.

One element is missing in the filter mechanization discussion, and that is any mechanization error due to finite computer word length or to algorithmic truncation in the navigation algorithm. These errors may be controlled to small values by proper design of the receiver computer algorithms.

4. NAVIGATION ACCURACY SIMULATION

This chapter presents the major results on the potential for utilizing a simple GPS receiver to navigate a NOSS spacecraft. The results derive mainly from a simulation of the orbital relationships involved and of the navigation filter assumed contained in the GPS receiver. In part, the results are based on past work relating to satellite navigation with GPS. There are three major sections in this chapter. The first deals with the orbit relationships that determine how many GPS satellite signals will be available for measurement and what the measurement geometry will be. The second section deals with the design of the navigation filter to process the measurements, although the technical details of the filter used for the simulation are placed in Appendix B. The third section summarizes the results of a covariance analysis of filter performance for two situations: one with 12 GPS satellites uniformly spread and one with four GPS satellites bunched into a test constellation.

4.1 GPS SATELLITE VISIBILITY

The ability to navigate using a GPS receiver depends on having an adequate number of GPS signals available. For a user with large dynamical uncertainties -- a high performance aircraft without an inertial navigation system, for example -- an adequate number of signals is generally four, a number commonly quoted as necessary. For a user with very low dynamical uncertainties -- a NOSS spacecraft, for example -- it is not necessary to have four GPS signals available simultaneously.

Nonetheless, there is some level of signal availability that will strongly impact navigation capability, and it is important to know both what that level is and what signal availability might be expected as various tradeoffs are made. This section deals with the issue of GPS signal availability.

Signal availability for radio communications systems generally involves considerations of transmitting power levels, transmitting antenna patterns, the distance from transmitter to receiver, interfering effects, receiver antenna gains, and other radio link margin factors. For near-earth GPS users, in particular for the NOSS spacecraft, most of these factors are irrelevant (Ref. 15). GPS satellites are so far from the earth, at 20,000 km altitude in their 12 hr orbits, that transmitter-to-receiver distances for near-earth users do not vary much. Transmitting antenna beamwidth is adequate to cover the entire near-earth region in the main lobe. GPS signals, having wavelengths of about 19 cm at the L1 frequency, travel in a line-of-sight fashion and are blocked by objects having dimensions comparable to a wavelength or larger, objects such as the earth itself or other obstructions near the receiving antenna. Transmitting power levels and processing gains are such that C/A-code acquisition will be possible for any signal coming from a GPS satellite visible to any part of the receiving antenna pattern with a gain of about -4 dBiC or more. Thus, GPS signal availability for NOSS is equivalent to satellite visibility.

There are four factors generally involved in satellite visibility:

- the GPS satellite constellation, i.e., the number of satellites and their orbit relationships
- the NOSS spacecraft orbit details

- the earth considered as a signal block
- the receiving antenna coverage.

The NOSS spacecraft will probably have a physical form resembling a large slab with the flat side always facing the earth, plus a large flat array of solar cells canted off to one side. The GPS antenna will in all likelihood be mounted on the side away from the earth and be limited by the slab itself to about a hemisphere of viewing. In such an arrangement, the earth would not be a factor in signal blockage. Even if the antenna field of view is not limited, signal paths below the satellite horizontal plane will probably be avoided due to the adverse effects on navigation accuracy of signal passage through the ionosphere. In any event, the receiving antenna is likely to be stabilized relative to the earth and to cover a conical segment centered about the zenith; hence, blockage of signal paths is not a prime consideration. The antenna coverage zone is henceforth assumed to extend from the zenith down to some limiting angle termed the "zenith angle limit," and this limit is treated parametrically.

The NOSS spacecraft is assumed to be in a nominally circular orbit at 70 to 110 deg inclination to the equator and at 600 to 800 km altitude. The right ascension of the NOSS orbit (equivalently, the longitude of the ascending node) is assumed to be unspecified. Most importantly, the time frame of interest begins in mid 1986 and extends for five years or so. The reason that the time frame is important is related to the GPS development schedule shown as Fig. 1-1. GPS is not expected to be fully operational until the end of 1987. Full operational capability is currently regarded to be a constellation of 18 navigation satellites, although the formerly planned constellation of 24 satellites is commonly found in GPS literature. Initial operational capability (compatible

with two-dimensional navigation capability for earth-bound users with independent knowledge of altitude) is scheduled for late 1985. About nine satellites are needed for this capability, although they may be made up of three to five of the Phase III satellites plus four to six of the Phase II development satellites still active at that time. By mid-to-late 1986 there should be about 12 satellites operational.

All of the orbit details for the Phase III operational GP$ constellation are not settled, but some features seem firm. The orbits will all be nominally circular at a common orbital inclination and a common altitude. The inclination is selected to be as high as practical with the launch system. The six satellites now in orbit as part of the Phase II development constellation are in 63 deg inclination orbits, but the Phase III satellites are to be launched by the Space Shuttle from the Cape Kennedy complex, most likely to 55 deg inclinations. The orbital altitude is selected so that the periods are 12 sidereal hours, so that the satellite ground tracks repeat once per day. (In fact, the periods are slightly adjusted to account for earth oblateness effects to keep the repeating ground tracks.) The altitudes are about 20,183 km.

The remaining orbital details are best discussed with reference to the original plans for the 24 satellite constellation. The 24 satellites were to be placed in three orbital planes uniformly spaced 120 deg apart in right ascension. The eight satellites in each plane were to be uniformly spaced by 45 deg in anomaly, and the set of anomalies were to be incremented by 15 deg from plane to plane. Table 4.1-1 shows a snapshot of right ascension and anomaly values for this uniform, 24 satellite constellation, taken with the #1 Satellite at the ascending node. The reference point for the right ascensions in the table is arbitrary for purposes here, as the NOSS

TABLE 4.1-1

ORIGINAL, 24 SATELLITE CONSTELLATION
INITIAL RIGHT ASCENSIONS AND ANOMALIES

ORBIT PLANE 1		ORBIT PLANE 2		ORBIT PLANE 3	
RIGHT ASC.	0 DEG	RIGHT ASC.	120 DEG	RIGHT ASC.	240 DEG
SAT. NO.	ANOMALY (DEG)	SAT. NO.	ANOMALY (DEG)	SAT. NO.	ANOMALY (DEG)
1	0	9	15	17	30
2	45	10	60	18	75
3	90	11	105	19	120
4	135	12	150	20	165
5	180	13	195	21	210
6	225	14	240	22	255
7	270	15	285	23	300
8	315	16	330	24	345

spacecraft orbit right ascension is unspecified and will be treated parametrically with respect to the satellite constellation.

One way to establish constellations of fewer than 24 satellites (as long as they number a multiple of three) is to spread the satellites uniformly in three orbit planes by increasing the anomaly spacing appropriately. This method is used for the visibility results reported here for constellations having a multiple of three satellites.

A second way to establish constellations of fewer than 24 satellites is to simply leave "holes" in the original pattern. This method results in a nonuniform constellation,

but one that is more simple to establish (as satellites need not be moved when additions are made) and that has room for non-operating spares. The "holes" would be chosen by omitting satellites whose earth-fixed, repeating ground tracks are largely over mid ocean areas.

This nonuniform method of establishing the constellation may seem particularly adverse for NOSS, which is primarily interested in ocean areas. As will be shown, however, satellite visibility with any reasonable 18 satellite constellation will lead to excellent navigation capability for NOSS, so the details of the full constellation are not very important. Navigation capability with the very nonuniform current test constellation of only four satellites will also be investigated to demonstrate the limits of performance.

A third method of establishing the 18 (or fewer) satellite constellations would increase the number of orbit planes to 6, 9, 18, or even 24 (with "holes"). This method limits multiple satellite launches, but is more resistant to anti-satellite activity, and may provide more uniform coverage than would leaving holes in the 24 satellite pattern.

In order to investigate visibility parametrically, a reference case is established and then varied. The reference case has the NOSS spacecraft at 90 deg orbital inclination at 700 km altitude. Visibility patterns are investigated for one orbital revolution of the NOSS spacecraft, from ascending node to ascending node. The reference case antenna has a zenith angle limit of 100 deg, selected because it is easily achievable (but later restricted on the basis of the ionospheric error studies). The GPS constellation for the reference case consists of twelve satellites, uniformly spread in three planes, as discussed above.

One aspect of the reference case requires an extended explanation. It involves a concept termed "offset time." At a time termed the NOSS epoch, the NOSS spacecraft is assumed to be at its ascending node, and that ascending node is assumed to be fixed in longitude relative to the earth. At some other time, up to one day later, termed the GPS satellite epoch, the #1 GPS Satellite is assumed to be at its "primary" ascending node (there are two nodes relative to the earth), and that node is also assumed to be fixed in logitude relative to the earth. The time span from the NOSS epoch to the GPS satellite epoch is called here offset time, and it is parameterized over a full span of one sidereal day. Without belaboring the point, it should be recognized that varying offset time varies the relationship of the NOSS orbit plane with respect to the GPS orbit planes as well as varying the positions of the GPS satellites within their planes for any time referenced to the NOSS epoch. The term "user time" in the visibility results is with respect to the NOSS epoch.

Given the variation in offset time, it might seem needless to also vary the initial longitude of the NOSS spacecraft ascending node (at the NOSS epoch) relative to that of the #1 GPS Satellite (at the GPS epoch). But this longitude variation changes the orbit plane relationships without also moving the satellites within their orbits, and represents an independent free parameter for the visibility studies. As will be shown, with uniformly spread satellite constellations of a dozen satellites or more, neither offset time nor initial longitude variations are important to satellite visibility.

An example of the detailed visibility output for the reference case is shown in Table 4.1-2. This table shows which of the twelve satellites are visible at each of 48, 7.5 deg steps in the travel of the NOSS spacecraft making one complete

TABLE 4.1-2

EXAMPLE VISIBILITY OUTPUT
(REFERENCE CASE, OFFSET TIME = 0)

R-61472

USER TIME (MIN)	TOTAL VISIBLE	SATELLITES 1	2	3	4	5	6	7	8	9	10	11	12
0.00	5	1	0	0	0	0	0	1	1	1	1	0	0
2.06	4	1	0	0	0	0	0	1	0	1	1	0	0
4.12	5	1	1	0	0	0	0	1	0	1	1	0	0
6.17	6	1	1	0	0	0	1	1	0	1	1	0	0
8.23	6	1	1	0	0	0	1	1	0	1	1	0	0
10.29	6	1	1	0	0	0	1	1	0	1	1	0	0
12.35	6	1	1	0	0	0	1	1	0	1	1	0	0
14.40	5	1	1	0	0	0	1	0	0	1	1	0	0
16.46	5	1	1	0	0	0	1	0	0	1	1	0	0
18.52	6	1	1	0	0	1	1	0	0	1	1	0	0
20.58	6	1	1	0	0	1	1	0	0	1	1	0	0
22.64	6	1	1	0	0	1	1	0	0	1	1	0	0
24.69	6	1	1	0	0	1	1	0	0	1	1	0	0
26.75	6	0	1	0	0	1	1	0	0	1	1	0	0
28.81	4	0	1	0	0	1	1	0	0	1	1	0	0
30.87	5	0	1	1	0	1	1	0	0	1	1	0	0
32.92	6	0	1	1	0	1	1	0	0	1	1	0	0
34.98	6	0	1	1	0	1	1	0	0	1	1	0	0
37.04	6	0	1	1	0	1	1	0	0	1	1	0	0
39.10	6	0	1	1	0	1	1	0	0	1	1	0	0
41.16	5	0	1	1	0	1	1	0	0	0	1	0	0
43.21	5	0	1	1	0	1	1	0	0	0	1	0	0
45.27	5	0	1	1	0	1	0	0	0	0	1	0	1
47.33	5	0	1	1	0	1	0	0	0	0	1	0	1
49.39	6	0	1	1	0	1	0	0	1	0	1	0	1
51.44	6	0	1	1	0	1	0	0	1	0	1	0	1
53.50	6	0	1	1	0	1	0	0	1	0	1	0	1
55.56	6	0	1	1	0	1	0	0	1	0	1	0	1
57.62	5	0	1	1	0	1	0	0	1	0	1	0	1
59.68	5	0	0	1	0	1	0	0	1	0	1	0	1
61.73	5	0	0	1	1	0	0	0	1	0	1	0	1
63.79	6	0	0	1	1	0	0	1	1	0	1	0	1
65.85	6	0	0	1	1	0	0	1	1	0	1	0	1
67.91	6	0	0	1	1	0	0	1	1	0	1	0	1
69.96	5	0	0	1	1	0	0	1	1	0	1	0	0
72.02	5	0	0	1	1	0	0	1	1	0	1	0	0
74.08	6	0	0	1	1	0	0	1	1	0	1	0	0
76.14	6	0	0	1	1	0	0	1	1	0	1	0	0
78.20	6	0	0	1	1	0	0	1	1	0	1	0	0
80.25	6	0	0	1	1	0	0	1	1	0	1	0	0
82.31	5	0	0	1	1	0	0	1	0	0	1	0	0
84.37	4	0	0	0	1	0	0	1	0	0	1	0	0
86.43	5	1	0	0	1	0	0	1	0	0	1	0	0
88.48	5	1	0	0	1	0	1	1	0	0	1	0	0
90.54	6	1	0	0	1	0	1	1	0	1	1	0	0
92.60	6	1	0	0	1	0	1	1	0	1	1	0	0
94.66	6	1	0	0	1	0	1	1	0	1	1	0	0
96.72	6	1	0	0	1	0	1	1	0	1	1	0	0

orbit. This detailed output is useful in making up realistic GPS measurement schedules for navigation performance simulations. The total number of satellites visible at each point in the NOSS orbit is also listed. As the table notes, these values are for an offset time of zero. That is, the #1 GPS Satellite and the NOSS spacecraft are at their respective ascending nodes at the same time. As offset time is varied, the visibility pattern changes. For this reference case, it does not change markedly, as the satellites are uniformly spread.

Fig. 4.1-1, termed a "visibility density plot," shows how the total number of satellites visible changes with offset time. The first column of the figure is taken directly from Table 4.1-2. As the figure shows, there are almost always four, five, or six satellites visible, the only exception being three occurrences of only three visible satellites. It might be noted that the columns of the figure repeat three times precisely. This is a feature of the uniform 12 satellite constellation not shared by most other constellations.

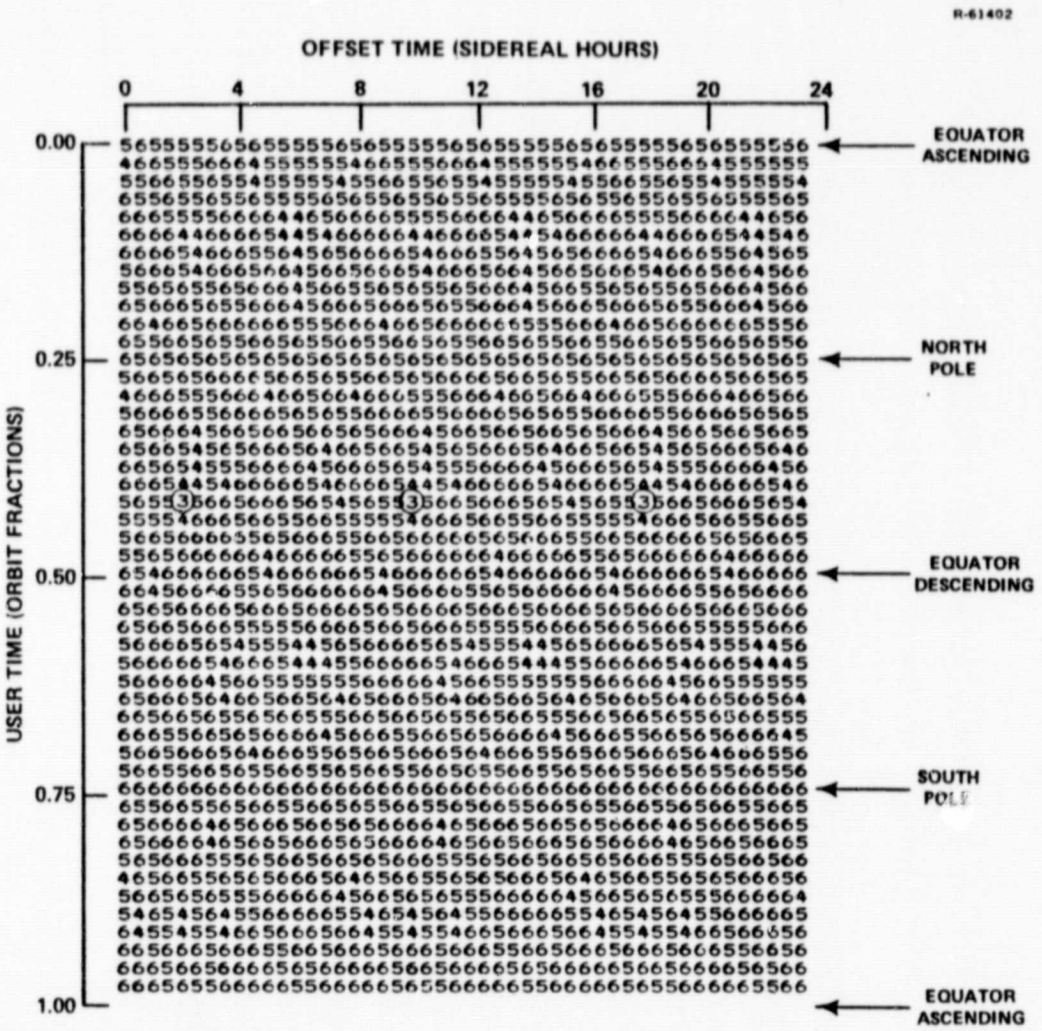

Figure 4.1-1 Reference Visibility Density Plot

Visibility statistics may be extracted from Fig. 4.1-1 by averaging over both time on orbit for the NOSS spacecraft and over offset time. When this is done, with the twelve satellite constellation it happens that exactly four satellites are visible 7% of the time, five are visible 36% of the time, and six are visible 57% of the time. On the average, 5.5 satellites are visible in the reference case.

Several of the variable parameters of the visibility situation have little or no impact on visibility. They include the initial longitude of the ascending node, the orbital inclination, and the altitude of the NOSS spacecraft (when limited to the ranges considered here). Tables 4.1-3, 4.1-4, and 4.1-5

TABLE 4.1-3
VISIBILITY VARIATIONS WITH USER INITIAL LONGITUDE

R-61473

USER INITIAL LONGITUDE OF ASCENDING NODE (DEG)	% OF TIME N SATELLITES ARE VISIBLE FOR N EQUALS				AVERAGE NUMBER OF SATELLITES VISIBLE
	3	4	5	6	
0		7	36	57	5.49
15	1	6	38	55	5.47
30		7	33	59	5.52
45		7	36	57	5.49
60	1	6	38	55	5.47
75		7	33	59	5.52
90		7	36	57	5.49
105	1	6	38	55	5.47

TABLE 4.1-4

VISIBILITY VARIATIONS WITH USER ORBITAL INCLINATION

R-61474

USER ORBITAL INCLINATION (DEG)	% OF TIME N SATELLITES ARE VISIBLE FOR N EQUALS				AVERAGE NUMBER OF SATELLITES VISIBLE
	3	4	5	6	
70	1	7	36	55	5.47
80	1	7	36	56	5.47
90	0	7	36	57	5.49
100	1	8	35	57	5.48
110	1	7	38	55	5.47

TABLE 4.1-5

VISIBILITY VARIATIONS WITH USER ORBITAL ALTITUDE

R-61475

USER ALTITUDE (km)	% OF TIME N SATELLITES ARE VISIBLE FOR N EQUALS			AVERAGE NUMBER OF SATELLITES VISIBLE
	4	5	6	
600	7	35	58	5.50
650	7	36	57	5.50
700	7	36	57	5.49
750	8	36	56	5.48
800	8	36	55	5.47

show the time variations in visibility with these parameters. The initial longitude was varied over 120 deg, the spacing between the GPS satellite orbit planes. Even over this limited range, a repeating pattern is noticed at 45 deg increments, equal to the anomaly spacing of the GPS satellites in an orbit plane. The limited range of NOSS spacecraft orbital inclinations produces no dramatic effect on visibility, nor does the limited range of orbital altitudes. Because the zenith angle viewing limits are held fixed in these results (at 100 deg) the higher orbital altitudes have slightly reduced visibility instead of the improved visibility one might expect as the spacecraft moves farther from the earth.

More significant are the visibility variations with the antenna zenith angle viewing limit and with the number of satellites in the constellation. Tables 4.1-6, 4.1-7, and 4.1-8 show the visibility variations with zenith angle limitations

TABLE 4.1-6

VISIBILITY VARIATIONS WITH ZENITH ANGLE LIMIT
(12 SATELLITE CONSTELLATION)

ZENITH ANGLE LIMIT (DEG)	% OF TIME N SATELLITES ARE VISIBLE FOR N EQUALS							AVERAGE NUMBER OF SATELLITES VISIBLE
	2	3	4	5	6	7	8	
80	11	38	40	11				3.52
85	4	25	42	27	2			3.98
90	1	13	36	41	9			4.45
95		4	20	49	26			4.97
100			7	36	57			5.49
105					99	1		6.01
110					55	37	8	6.53

TABLE 4.1-7

VISIBILITY VARIATIONS WITH ZENITH ANGLE LIMIT
(15 SATELLITE CONSTELLATION)

ZENITH ANGLE LIMIT (DEG)	% OF TIME N SATELLITES ARE VISIBLE FOR N EQUALS									AVERAGE NUMBER OF SATELLITES VISIBLE
	2	3	4	5	6	7	8	9	10	
80	2	13	37	41	8					4.40
85		3	23	46	27					4.97
90			8	28	60	3				5.58
95			2	9	58	27	3			6.20
100				2	32	47	18	2		6.85
105					10	39	40	11		7.51
110					1	17	46	33	2	8.18

TABLE 4.1-8

VISIBILITY VARIATIONS WITH ZENITH ANGLE LIMIT
(FULL, 18 SATELLITE CONSTELLATION)

ZENITH ANGLE LIMIT (DEG)	% OF TIME N SATELLITES ARE VISIBLE FOR N EQUALS									AVERAGE NUMBER OF SATELLITES VISIBLE
	4	5	6	7	8	9	10	11	12	
80	20	35	40	4						5.28
85	8	18	47	24	3					5.97
90	3	7	30	41	18	2				6.69
95	1	2	12	37	37	42				7.44
100			1	14	42	42				8.23
105						99	1			9.01
110						39	43	15	2	9.81

for 12, 15, and 18 satellite constellations. The important thing to note here is that even for an 80 deg zenith angle limit and a 12 satellite constellation, two or more satellites are always visible, and three or more are visible about 90% of the time. As will be shown, such visibility is quite adequate for NOSS spacecraft navigation.

Two specific visibility situations were used to generate navigation performance results. One is very nearly the reference case discussed above, except that a more conservative 85 deg zenith angle limit was assumed instead of the 100 deg limit of the reference case. The other situation selected for navigation performance simulation is a minimal visibility situation involving a very non-uniform constellation of only four GPS satellites, an approximation to the current test constellation.

Figure 4.1-2 shows, in a new format, the detailed visibility results for the 12 satellite case used for navigation performance simulation. The presence of a bar indicates that a satellite is visible within the 85 deg zenith angle viewing limit assumed for the receiver antenna. This figure bears a very close relationship to Table 4.1-2, which is for the same situation except that the antenna viewing limit is 100 deg. Tic marks have been added to the figure to show the measurement schedule used for the navigation performance simulation. One measurement (or measurement pair) is assumed each minute, and, beginning with Satellite #1 at time zero, the receiver is assumed to select for measurement the next satellite in numerical order that is visible, cycling from Satellite #12 back to Satellite #1.

In practice, even a single channel receiver could probably make a measurement (or measurement pair) every three

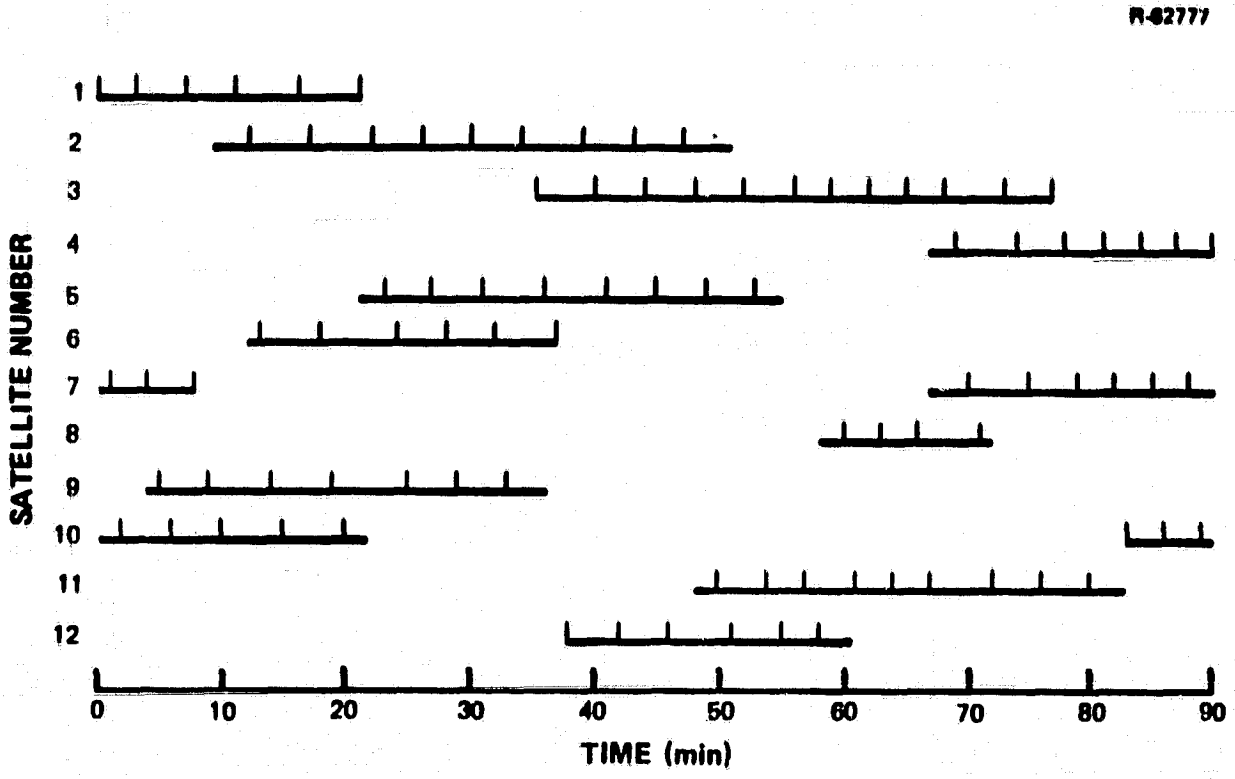

Figure 4.1-2 Satellite Visibility and Measurement Schedules - 12 Satellite Constellation

to six seconds, except that the first measurement after a satellite becomes visible would require an additional delay of about 30 sec to gather the navigation data from the signal. The faster measurement rate serves to reduce the effect of uncorrelated noise (white noise) in the measurements, but it does little or nothing to abate correlated measurement errors (biases). The navigation performance simulation does not include some known, if small, sources of correlated error (e.g., satellite ephemeris and clock, ionospheric delays). The slower, simulated measurement rate in conjunction with properly chosen measurement variances compensates for this simplification, at least for error sources whose correlation time is of the order of the time span between measurements to a particular satellite, a few minutes.

One other difference due to measurement rates is the transient response of the filter. If navigation errors are initially high or have grown large after a period of no GPS measurements, the immediate recovery is generally a function only of the number of measurements taken to different satellites. Of course, with a single channel receiver, it takes 35 sec or so to make each measurement to a new satellite after a period of no visibility, so the actual transient recovery periods could be somewhat shorter than those shown in the simulation results, possibly by about 50%.

Figure 4.1-3 shows the detailed visibility results and measurement schedule for the four satellite test constellation. No satellites are visible between 50 and 90 minutes, and a total period of 120 min is simulated to demonstrate a typical error recovery after such a visibility outage. The constellation used to generate these results is not one of those discussed earlier, but is an approximation to the current test constellation. The satellites are all in 63 deg (rather than 55 deg) inclination orbits, and the initial right ascensions and anomalies are shown in Table 4.1-9.

R-62776

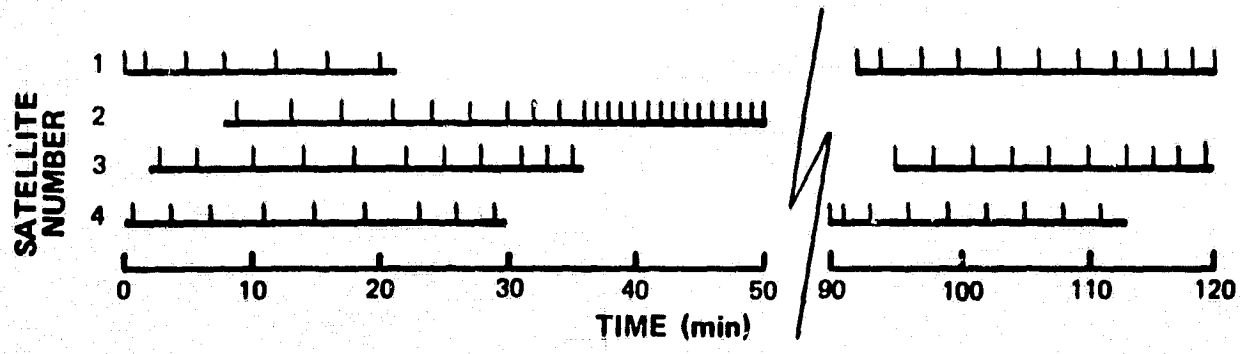

Figure 4.1-3 Satellite Visibility and Measurement Schedule - Four Satellite Constellation

TABLE 4.1-9
INITIAL CONDITIONS FOR
THE FOUR SATELLITE CONSTELLATION

ORBIT PLANE 1		ORBIT PLANE 2	
RIGHT ASC.	0 DEG	RIGHT ASC.	240 DEG
SAT. NO.	ANOMALY (DEG)	SAT. NO.	ANOMALY (DEG)
1	0	3	75
2	90	4	120

Except for the GPS constellation, all the other details of this visibility situation are identical to those of the 12-satellite case. That is, the NOSS spacecraft is in a 90 deg inclination, 700 km circular orbit, initially over the equator directly under the #1 Satellite, and the receiving antenna has a zenith angle limit of 85 deg.

4.2 RECEIVER NAVIGATION FILTER

There are two different ways to turn GPS measurements into navigation data outputs. One way is to make four simultaneous measurements of pseudo range (or of pseudo range-rate) to four different GPS satellites and then to deterministically solve for three components of user position and for user clock phase error (or for three components of velocity and for user clock frequency error). The other way is to implement a navigation filter that acknowledges all the important, time-correlated states of the system impacting on the measurements and then update a running estimate of these states based on individual measurements as they are received. For a GPS user with low dynamic uncertainties, such as a NOSS spacecraft, the

filter approach is clearly superior. For a user with a sequential receiver incapable of making simultaneous measurements, or for a user with access to fewer than four GPS satellites at once, the filter approach is all but essential.

A GPS pseudo range measurement generally contains information about all three components of user position and about user clock phase. A GPS pseudo range-rate (or delta range) measurement generally contains information about all three components of user velocity, all three components of user position, and about user clock frequency. A navigation filter to process these measurements should include at a minimum the eight user states involved: three components of position, three components of velocity, clock phase, and clock frequency. If only pseudo range measurements were to be used, it would still be advisable to use all eight states mentioned, as dynamical noise in the process tends to enter at the acceleration (aging) level, driving velocity (frequency) which in turn drives position (phase). If only pseudo range-rate measurements were to be used, there would be no navigational reason to include the clock phase state in the filter, as it would be unobservable. Operation of the receiver in its acquisition mode, however, would require some estimate of clock phase to be made, even if it were isolated from the navigation data output.

There are additional sources of correlated "errors" in the measurements, and the filter could acknowledge these. Included in this category are user dynamical uncertainty sources such as gravitational modeling errors, solar radiation pressure errors, and air drag errors. Also included in this category are the errors in GPS satellite navigation data pertaining to position, velocity, and the satellite clock. Finally, correlated signal transmission errors due to ionospheric effects could also be included, as could any receiver tracking loop

errors with significant correlation times. If any additional data is being used by the navigation filter (data from an altimeter for example) then correlated errors associated with that data source could also be acknowledged by the filter.

For moderate navigation accuracy for the NOSS application, it does not appear justifiable to include any but the basic eight states in the filter design. The improvements obtainable in navigation accuracy by modeling the other effects in the filter directly are not significant,* while the additional filter complexity generally is significant. Some adjustment of the filter will be necessary to account for dynamical noise coming from the small uncertainties in spacecraft acceleration, or else the filter will become overconfident of its ability to predict the vehicle position and velocity based on past information. It will then deweight or reject GPS measurement information, and its navigation outputs will diverge from the truth. But the adjustment to the filter to prevent this overconfidence need not take the form of explicitly modeling the acceleration uncertainties. Directly adding "noise" to the filter estimate of velocity error statistics will suffice.

Nonetheless, the version of the filter used for the simulation reported here does explicitly include error models for gravitational constant uncertainty, solar radiation pressure uncertainty, and for air drag acceleration uncertainty. The filter is not allowed to improve its knowledge of these effects through the measurement process; they are simply retained as a high-fidelity way to put dynamical noise into the filter.

*A possible exception might be the gravitational constant uncertainty state in situations with lengthy measurement gaps.

For purposes of evaluating the performance of the navigation filter, it would be desirable to model explicitly every correlated error source. GPS satellite navigation data errors and ionospheric signal propagation errors will have an impact on the results, even if it is not a large one. These effects are difficult to model well. The GPS satellite navigation data errors require a large number of states to model, from eight to twelve for each satellite in the constellation plus states to simulate the ground tracking segment of the system, adding from 50 to 200 states to the covariance simulation. Satellite navigation data errors are modeled in some past TASC studies of satellite-to-satellite navigation with GPS (Ref. 12), but such modeling is beyond the scope of this study. Ionospheric errors are difficult to model because the ionosphere and its variations are themselves complex, and because the essential effects are spatially as well as temporally correlated. Fortunately, there are a number of ways that potentially large ionospheric errors may be avoided. The effects of ionospheric errors and, to some extent, of GPS satellite ephemeris and clock errors may be accommodated in the simulation by reducing the measurement frequency and by adjusting the measurement noise variances. This was done.

There are a number of practical details very important to the implementation of an actual navigation filter in flight software. These include considerations of memory sizing, throughput capability, factorization of the basic algorithms, data editing and rejection, word length, truncation, etc. These factors have not been considered in the covariance simulation, because with proper design they are of negligible effect. Some analysis and simulation ultimately will be required to establish the limits of proper design.

Most of the details of the filter used for the navigation performance simulation are to be found in Appendix B.

The filter has eleven states: the basic eight plus the three acceleration uncertainty states. Since the filter is not allowed to update the acceleration uncertainty states, however, it behaves like the simpler, eight-state filter.

The navigation covariance estimates used to initialize the filter are not very important. For simulation purposes, the filter is initialized with independent errors of 500 m in each position error component and in clock phase error. (In all the numerical discussions of filter performance, the error values are statistical RMS or one sigma values, and clock errors are converted into equivalent position and velocity errors by multiplying time and frequency errors by the speed of light.) Independent values of 10 mps are used to initialize each velocity error component and clock frequency errors.

The measurement error variances assumed are 10 m for pseudo range and 0.025 mps for pseudo range-rate. These are reasonably conservative values for single frequency, C/A-code operation. While these errors are modeled as uncorrelated noises on the measurements, the simulated measurement schedule of but one measurement pair (pseudo range and pseudo range-rate) per minute (one per few minutes to a given satellite) allows the measurement variances to account for correlated errors with time constants of a few minutes. Some of the bias effects of ionospheric and GPS satellite ephemeris errors may thus be included, while at the same time, the truly uncorrelated components are reduced.

Additional numerical details of the filter associated with the clock and with the acceleration uncertainties are found in Appendix B. In summary, the gravitational constant uncertainty is assumed to be equivalent to a very conservative 3 μg's, the solar radiation pressure uncertainty is equivalent

to a small, but realistic, 0.0009 μg's, and the air drag uncertainty equivalent to an even smaller 0.0003 μg's. The clock is modeled to approximate a medium quality quartz crystal oscillator with a 3.3 parts in 10^{10} fractional frequency error over averaging periods from 1 to 20 min.

4.3 NAVIGATION PERFORMANCE SIMULATION RESULTS

The first navigation performance simulation results to be presented are those for the 12 satellite constellation with the visibility situation and measurement schedule previously given in Fig. 4.1-2. At each measurement time, a pair of measurements is assumed made, one of pseudo range and one of pseudo range-rate. The navigation results for the eight basic filter states are summarized in Figs. 4.3-1 through 4.3-4. While the navigation filter actually uses inertial components of position and velocity, the figures plot radial, along track, and cross track components because orbital error propagation is more easily understood and interpreted in these coordinates. The initial errors of 500 m and 10 mps are off the scales of these plots.

After processing measurements to four different satellites (the fourth satellite first appearing at 6 min) the navigation errors fall to below 25 m and 0.1 mps. As more measurements are made, especially to different satellites and to satellites whose geometry with respect to the user has changed significantly through time, the navigation errors continue to fall to about the assumed level for single measurement errors: 10 m and 0.025 mps. This is a better result than might be expected based on the usual considerations of Geometric Dilution of Precision (GDOP), that predict navigation errors to be somewhat larger, by perhaps a factor of two. The concept of GDOP

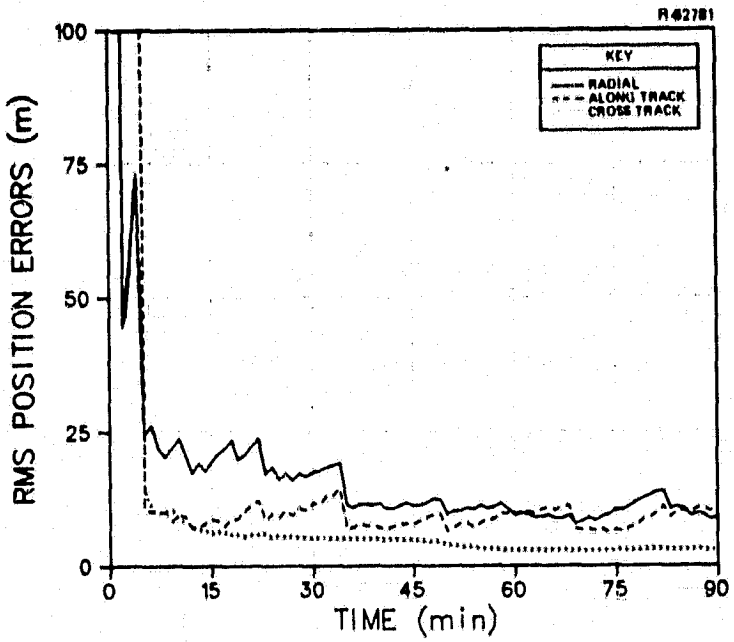

Figure 4.3-1 RMS Position Error, 12 Satellite Case, Both Pseudo Range and Pseudo Range-Rate Measurements

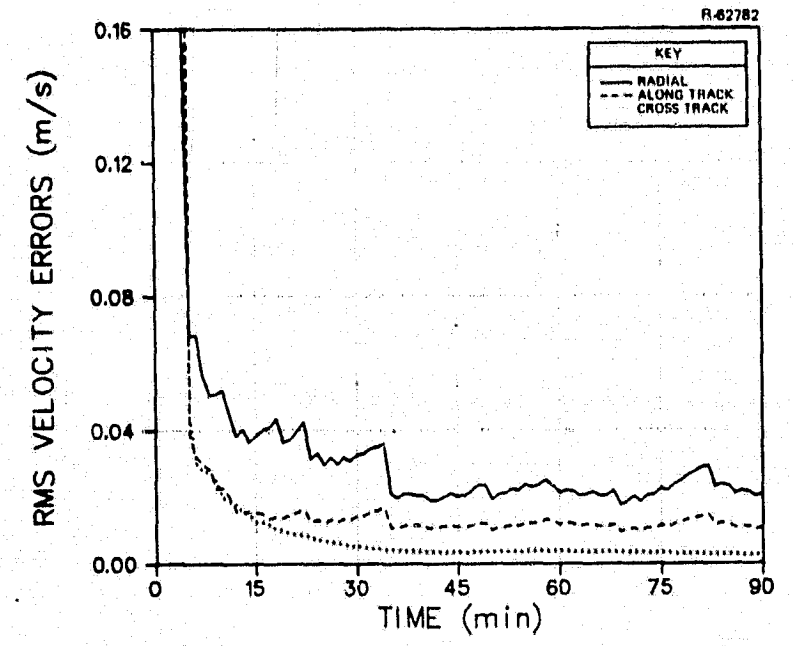

Figure 4.3-2 RMS Velocity Errors, 12 Satellite Case, Both Pseudo Range and Pseudo Range-Rate Measurements

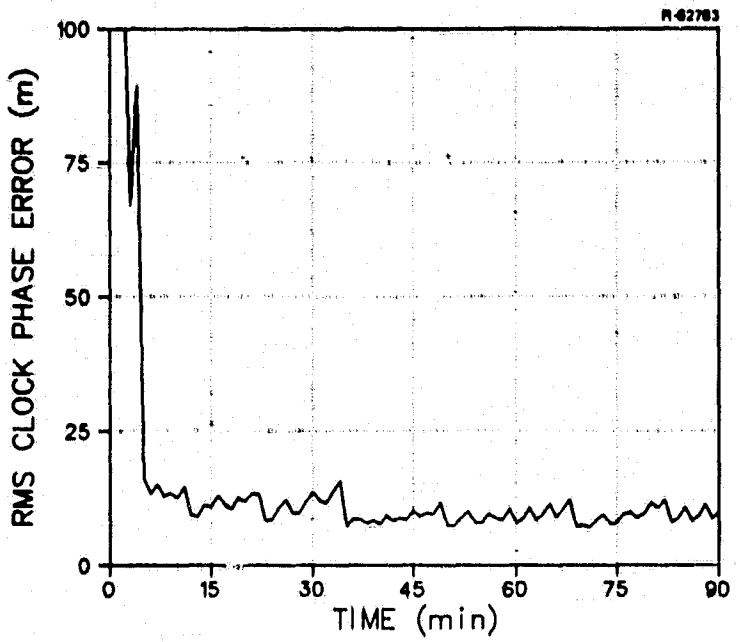

Figure 4.3-3 RMS Clock Phase Error, 12 Satellite Case, Both Pseudo Range and Pseudo Range-Rate Measurements

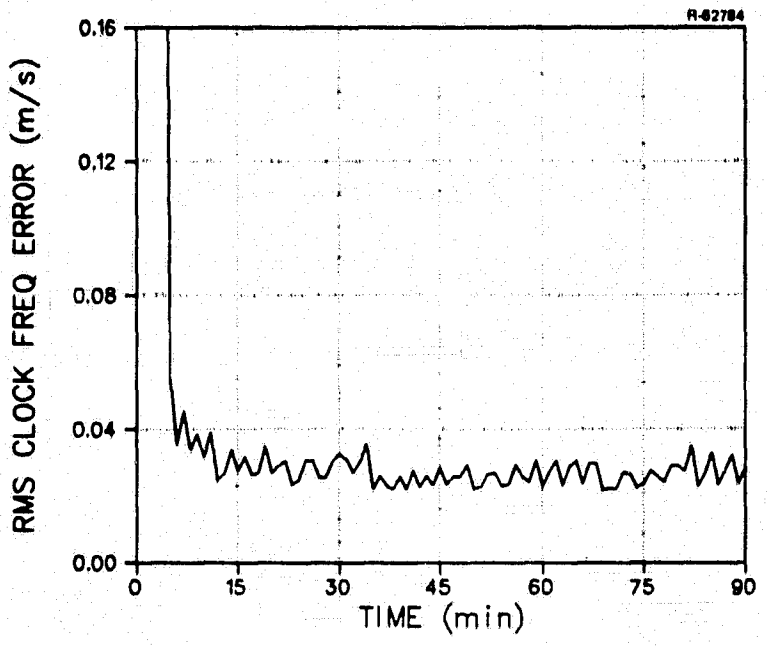

Figure 4.3-4 RMS Clock Frequency Error, 12 Satellite Case, Both Pseudo Range and Pseudo Range-Rate Measurements

does not strictly apply to the situation at hand -- using a Kalman filter to navigate a vehicle with very low acceleration uncertainties -- that allows many more than four measurements to influence the "steady state" results. GDOP is more applicable to the situation after only four satellites are first seen, and the simulation results are in tune with GDOP predictions.

Since two types of measurements are being made, pseudo range and pseudo range-rate, it is natural to wonder to what extent the filter is drawing its conclusions from one type or the other. Pseudo range measurements relate to position and clock phase errors, while pseudo range-rate measurements relate to velocity and clock frequency errors as well as to position errors. It might be expected that the filter would depend heavily on pseudo range measurements for position and phase accuracy, and upon pseudo range-rate measurements for velocity and frequency accuracy. There is some limited truth to this conclusion, but it depends on the relative sizes of the measurement standard deviations for the two types of measurements.

Figures 4.3-5 through 4.3-8 show that using pseudo range measurements alone is about equivalent to using both types of measurements, except that the transient error reduction is slowed somewhat, and the clock frequency error level remains higher. Figures 4.3-9 through 4.3-11 show that using pseudo range rate measurements alone produces some degradation in all estimates. Of course, clock phase is omitted here because it cannot be estimated at all with only pseudo range-rate measurements. The position estimates are degraded by a factor of two, while the velocity and clock frequency errors are only slightly worse than when both types of measurements are used.

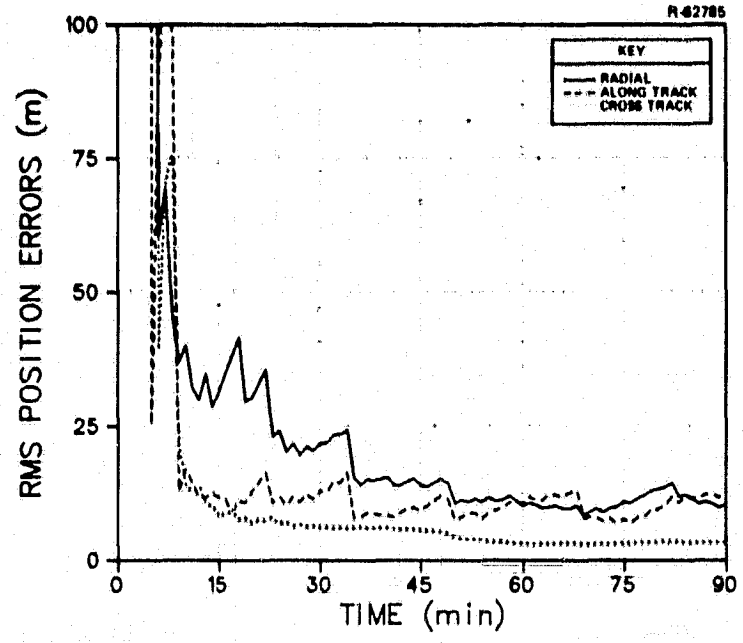

Figure 4.3-5 RMS Position Errors, 12 Satellite Case, Pseudo Range Measurements Only

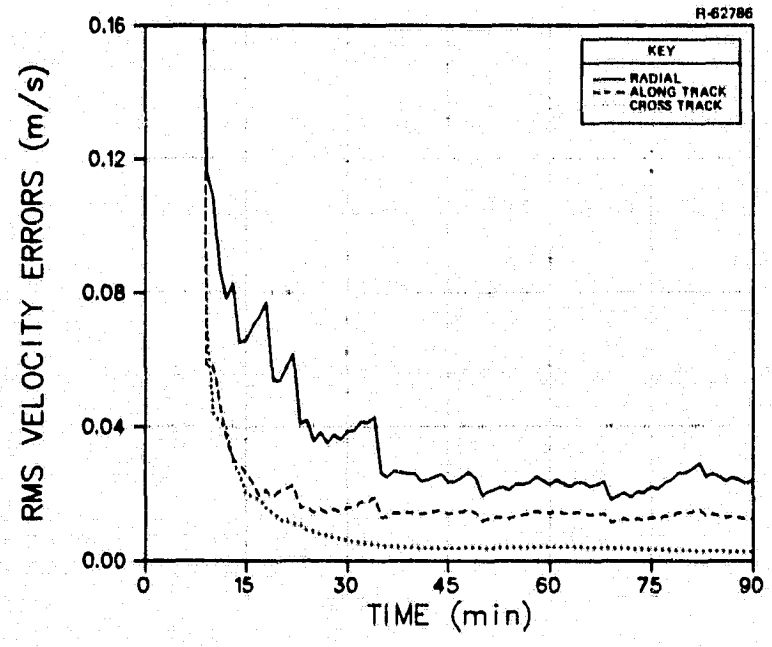

Figure 4.3-6 RMS Velocity Errors, 12 Satellite Case, Pseudo Range Measurements Only

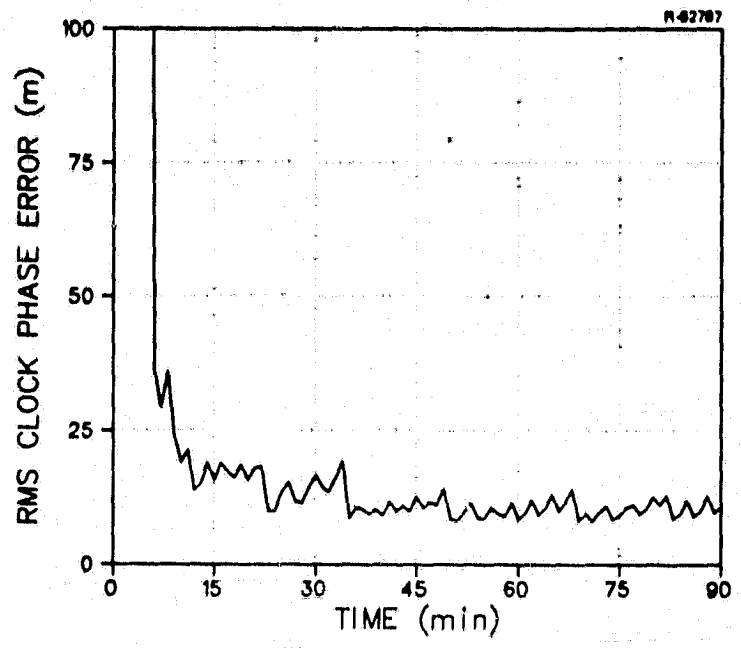

Figure 4.3-7 RMS Clock Phase Error, 12 Satellite Case, Pseudo Range Measurements Only

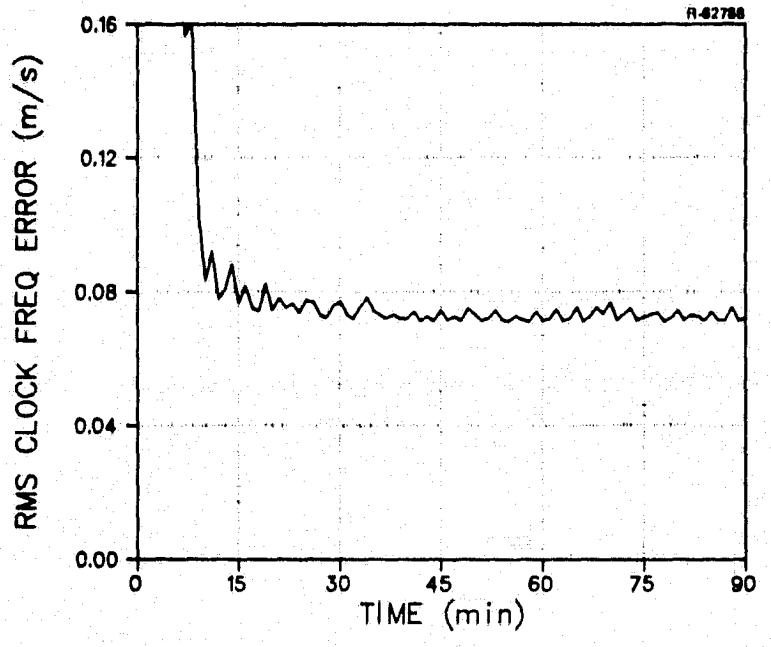

Figure 4.3-8 RMS Clock Frequency Error, 12 Satellite Case, Pseudo Range Measurements Only

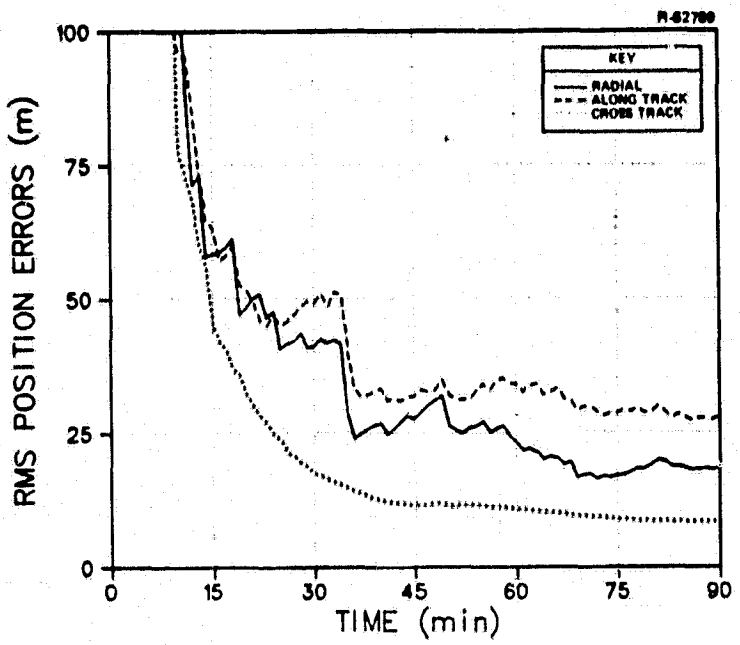

Figure 4.3-9 RMS Position Errors, 12 Satellite Case, Pseudo Range-Rate Measurements Only

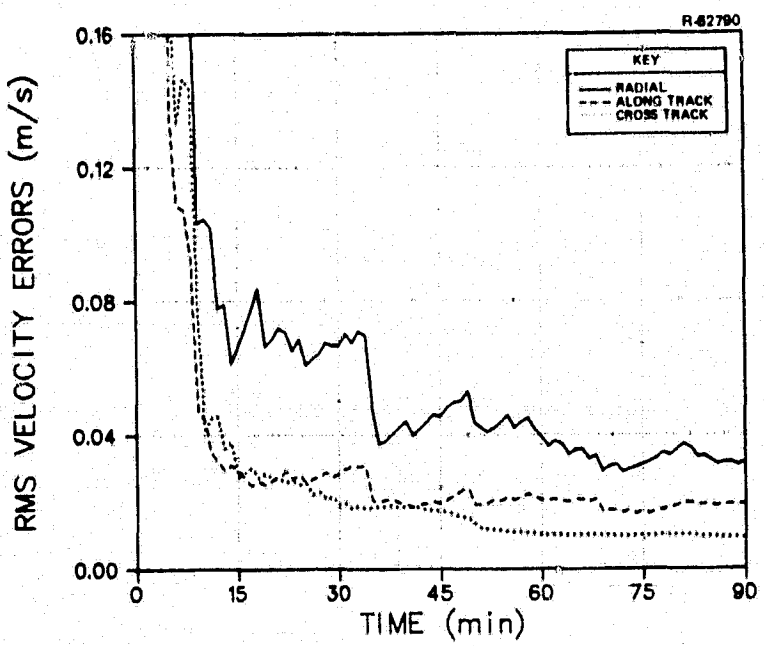

Figure 4.3-10 RMS Velocity Errors, 12 Satellite Case, Pseudo Range-Rate Measurements Only

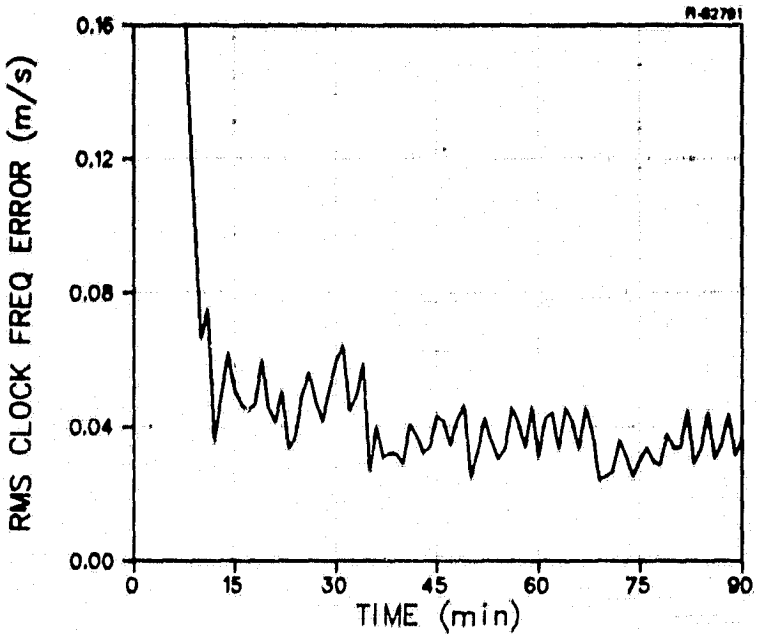

Figure 4.3-11 RMS Clock Frequency Error, 12 Satellite Case, Pseudo Range-Rate Measurements Only

As stated above, these single measurement type results depend strictly on the relative sizes of the measurement standard deviations. The plots for the single measurement types are of more than academic interest. They show how the results are sensitive to changes in assumptions about measurement errors. Within reason, the single measurement type results may be linearly scaled with the measurement standard deviations, to determine navigation sensitivity to a reduction (or increase) in the assumed measurement accuracies. In this case, the better result for either single measurement type will probably dominate the results when both measurement types are used.

The assumptions here for pseudo range-rate errors (a standard deviation of 0.025 mps) are very conservative. It might be possible by proper receiver design and by using a long enough doppler processing interval (perhaps several seconds) to reduce this value by a factor of three or even more. In

such a case, the pseudo range-rate measurements would dominate the results, the range measurements would be relatively unimportant, and the results could be estimated by simply scaling Figs. 4.3-9 through 4.3-11 by a factor of three or more reduction. It should also be noted that pseudo range-rate errors are generally much less sensitive than are pseudo range errors to ionospheric signal propagation effects, so depending only on pseudo range-rate measurements is one way to overcome adverse ionospheric problems associated with single frequency or single channel or C/A-code only operation.

The remaining navigation performance simulation results to be presented are those for the minimum visibility, four satellite constellation, with visibility details and measurement schedule previously given in Fig. 4.1-3.

Figures 4.3-12 through 4.3-15 show the simulation results for this case. Note the expanded scales over those used for the 12 satellite case. Note also the characteristic orbital error growth between about 35 and 90 min. After 35 min in this case, only one GPS satellite is visible. It disappears at 50 min, and none are seen again until 90 min. (This behavior is due to the fact that the four satellites of the test constellation are bunched so that all four may be seen simultaneously for test purposes for a few hours each day from some regions.) Along track position error and radial velocity error grow markedly when no satellites are in view. They grow in a highly correlated manner, so that but two GPS measurements to different satellites are sufficient to reduce the errors back to about their minimum values. Two GPS measurements are required, rather than one, because the clock errors also grow when no measurements are taken.

Figures 4.3-16 through 4.3-19 show the results of restricting to measurements of a single type for the four

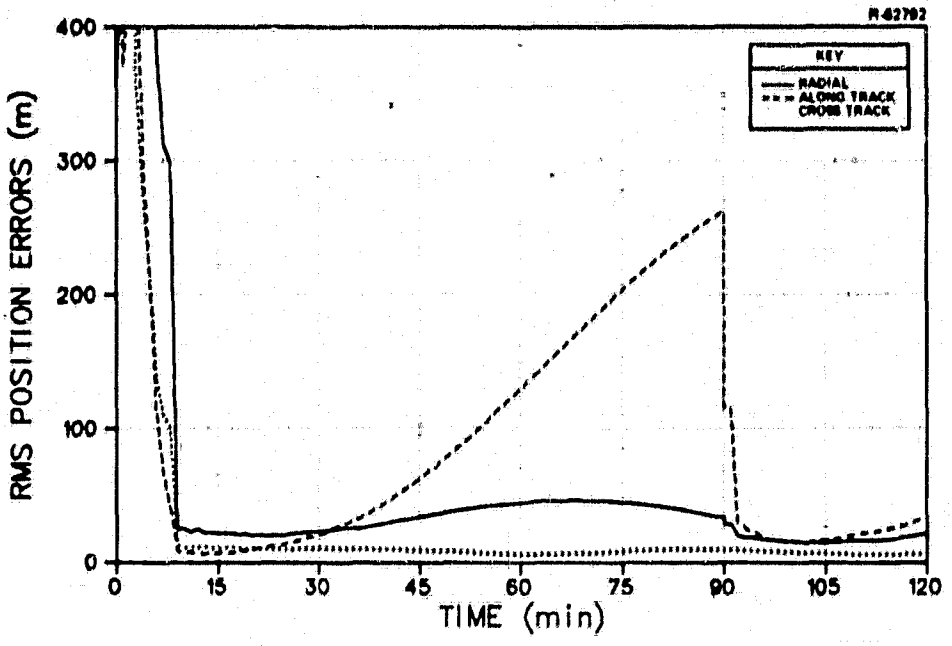

Figure 4.3-12 RMS Position Errors, Four Satellite Case, Pseudo Range and Pseudo Range-Rate Measurements

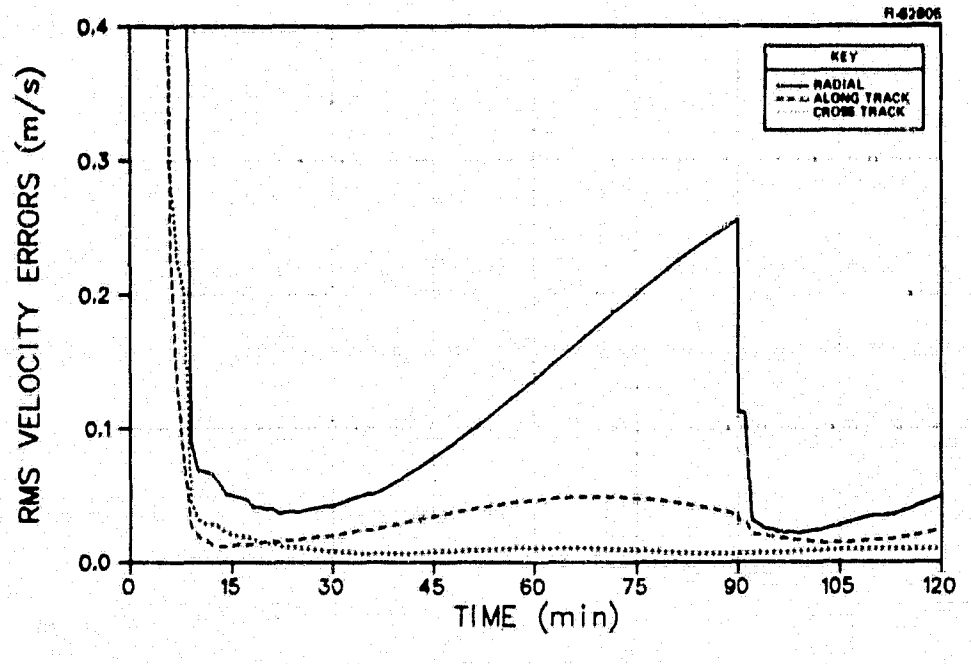

Figure 4.3-13 RMS Velocity Errors, Four Satellite Case, Pseudo Range and Pseudo Range-Rate Measurements

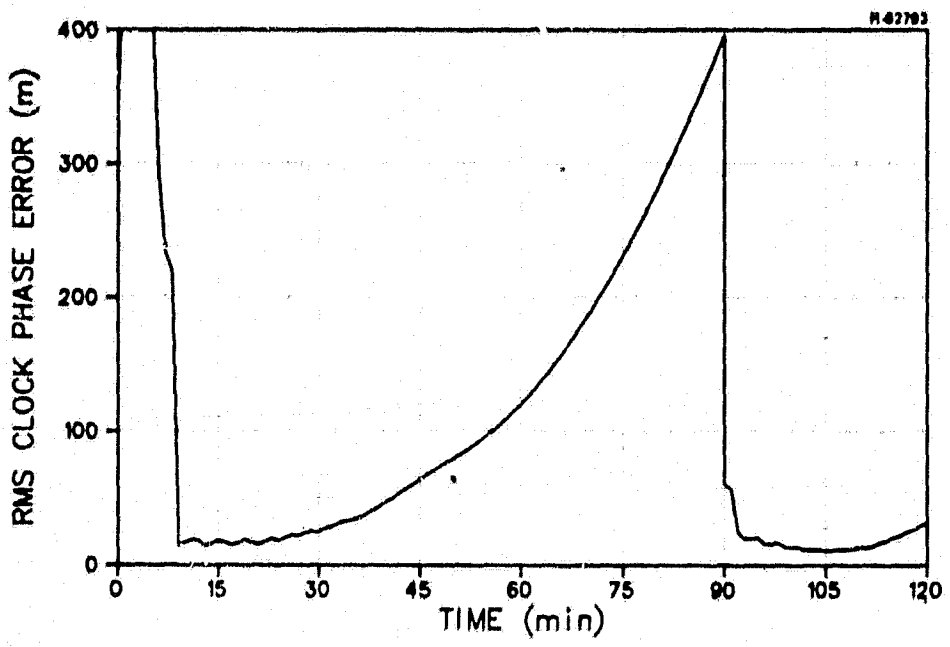

Figure 4.3-14 RMS Clock Phase Error, Four Satellite Case, Pseudo Range and Pseudo Range-Rate Measurements

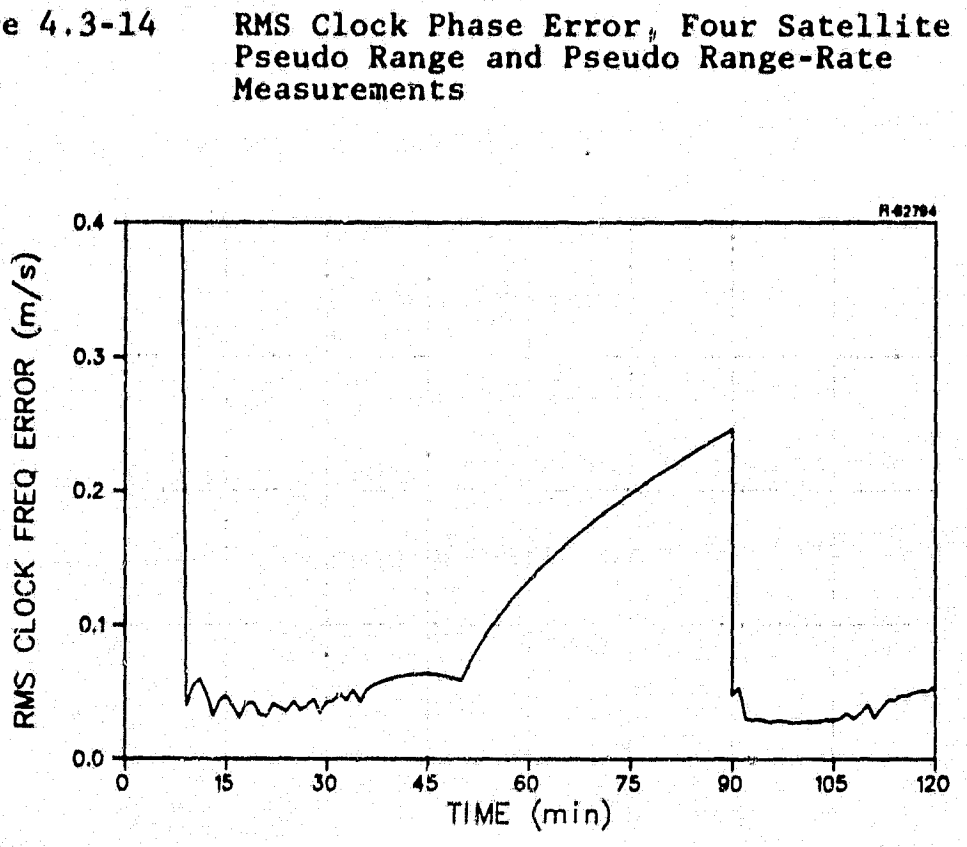

Figure 4.3-15 RMS Clock Frequency Error, Four Satellite Case, Pseudo Range and Pseudo Range-Rate Measurements

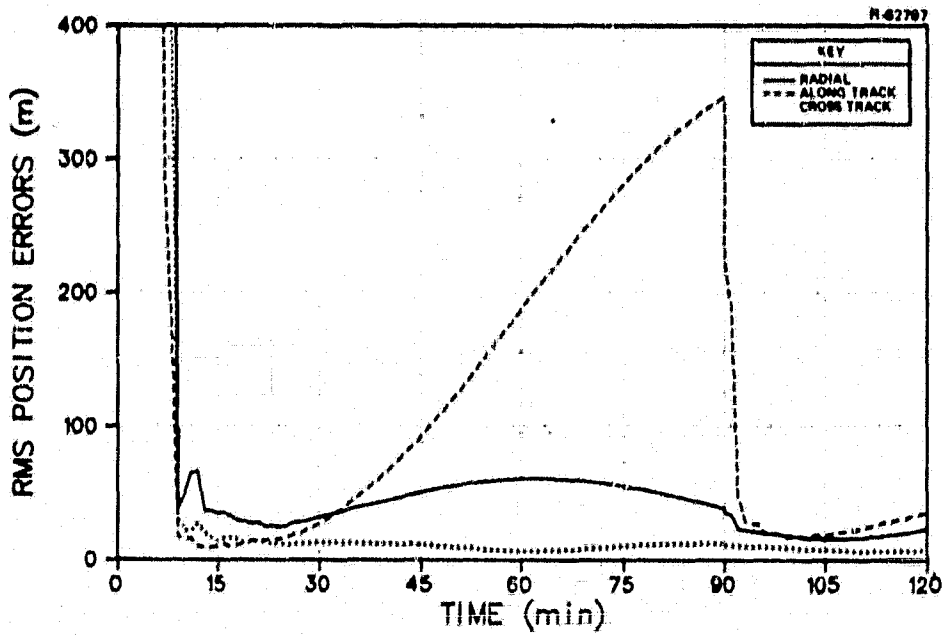

Figure 4.3-16 RMS Position Errors, Four Satellite Case, Pseudo Range Measurements Only

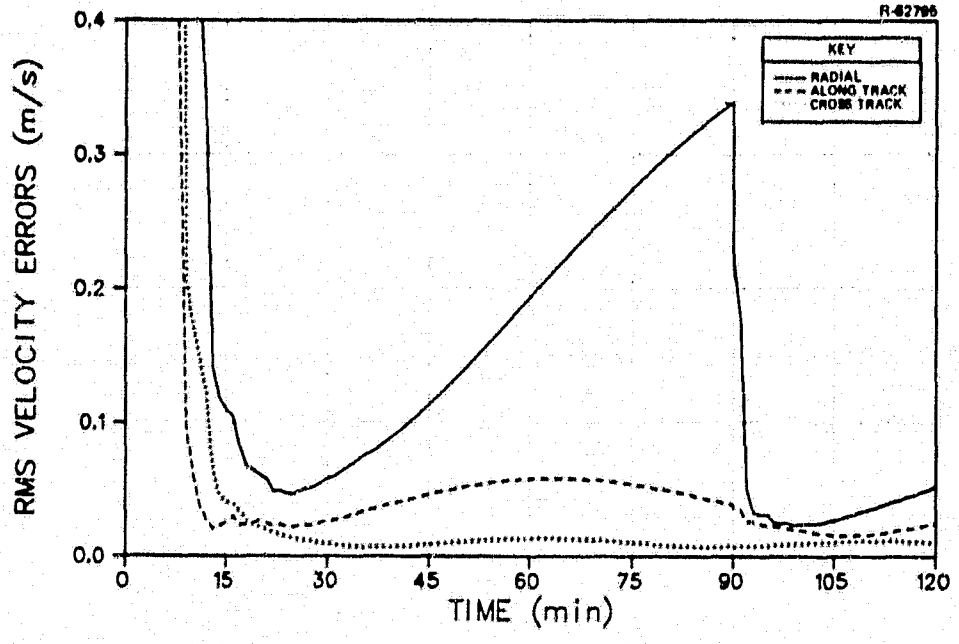

Figure 4.3-17 RMS Velocity Measurements, Four Satellite Case, Pseudo Range Measurements Only

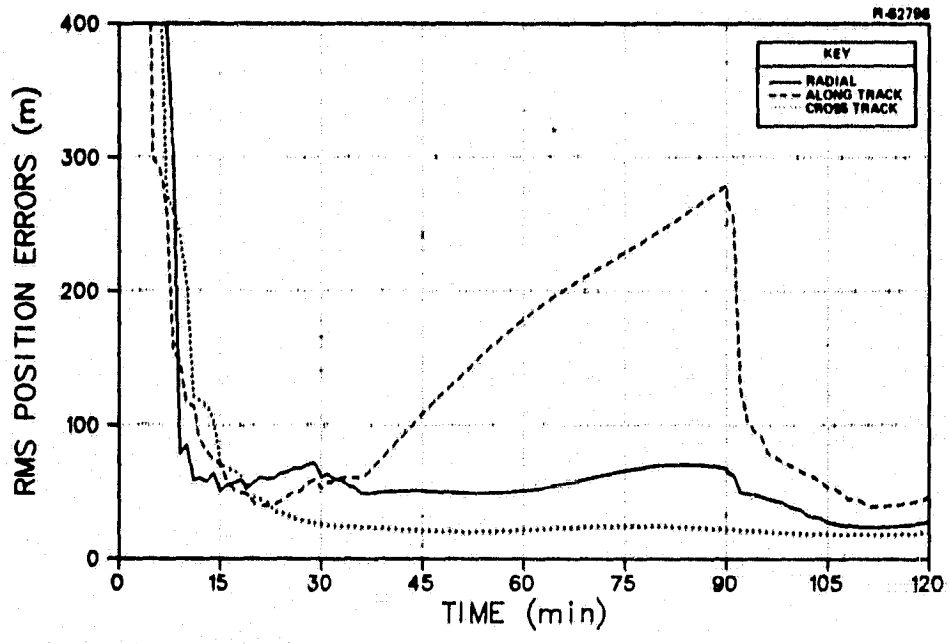

Figure 4.3-18 RMS Position Errors, Four Satellite Case, Pseudo Range-Rate Measurements Only

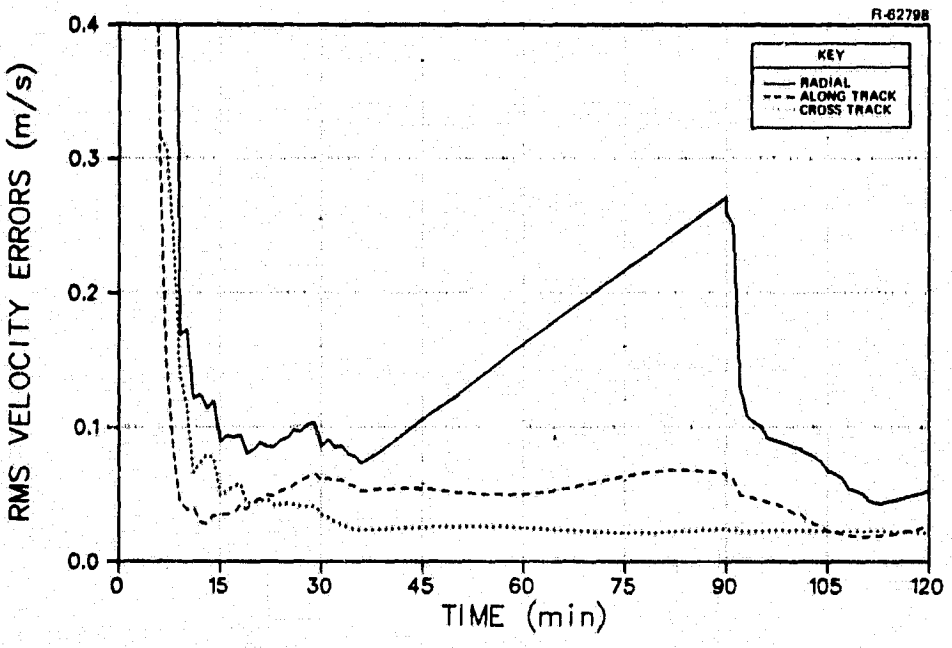

Figure 4.3-19 RMS Velocity Errors, Four Satellite Case, Pseudo Range-Rate Measurements Only

satellite case. The clock errors have been omitted. These results may be used to consider the sensitivity of the overall measurement process to variations in the standard deviations of the pseudo range and pseudo range-rate measurements in a manner similar to that just discussed for the 12 satellite case.

5. PRECISION RELATIVE ALTITUDE DETERMINATION

A NOSS mission goal is to enable vertical displacment of the NOSS spacecraft to be measured to a precision of 5 cm or better over an orbital arc of 500 km or more. The vertical precision requirement of 5 cm is two orders of magnitude lower than the usually quoted 5 m accuracy level of GPS; but there are several unusual features of the NOSS application that are not factored into the usual accuracy quotes:

- It is vertical displacement -- changes in altitude -- that are to be measured and not the absolute altitude itself.
- Limited variations in NOSS spacecraft-to-GPS satellite geometry are to be considered. The 500 km tracking arc goal for the NOSS spacecraft corresponds to no more than 67 sec of time at the maximum 800 km altitude.
- The NOSS spacecraft is in a very benign dynamical environment where uncertainties in acceleration may be less than 1 μg. If initial velocity were known exactly, 1 μg of acceleration error would cause only 2.2 cm of position error in 67 sec.
- The NOSS spacecraft is at an altitude where, with some limitation of satellite viewing angles, ionospheric and tropospheric effects on signal propagatation may usually be negligible.
- The estimates of vertical displacement need not be made in real time, a post arc ground processing environment is possible.

This chapter contains a study of the feasibility of obtaining such precision from GPS.

An important issue in addressing the problem of estimating vertical displacement is one of mechanization. The question is whether GPS can somehow meet the 5 cm NOSS accuracy goal, but the mechanization -- what data is to be gathered, and how it is to be processed -- is unspecified. As will be shown, there are certain inexorable error relationships that hold regardless of the mechanization. The most important of these is a connection between relative vertical displacement error and absolute spacecraft positioning errors in all directions. Before demonstrating this result, consideration will be given to the basic measurements.

Any method for utilizing GPS to reach the 5 cm accuracy goal for vertical displacement will undoubtedly involve making use of what are termed "delta range" measurements. A delta range measurement is a change in pseudo range measured while the receiver is tracking the carrier of the GPS signal without cycle slips. At the L1 frequency, the carrier wavelength is about 19 cm, and the carrier phase may be resolved to about 1/64 of a wavelength, or 2.5 mm. After a tracking time period larger than the inverse of the carrier loop bandwidth (typically 20 Hz), the phase errors at the beginning and end of the measurement period tend to become uncorrelated. As reported in Chapter 3 (for C/A-code, but the same result applies to P-code) the receiver phase measurement error is about 6 mm. Thus, depending on the mechanization, receiver measurement error need not be a limiting error source.

Changing ionospheric delays during the delta range measurement interval also add errors. Even for earth-based users, measurements of the ionospheric effects are less than 2 cm over a 1 min period (Ref. 23). Space-based users experience more rapid changes in geometry but see through much less (and much more stable) ionosphere.

Recent experimental investigations on GPS doppler processing at the Naval Surface Weapons Center (NSWC) in Dahlgren, Va. indicate that the basic stability of the satellite signals, the ionospheric corrections, and the receiver is sufficient to support the NOSS vertical displacement measurement goal (Refs. 23, 24). In the NSWC study, a GPS receiver in a van was used to make contiguous delta range measurements with 1 minute doppler processing intervals. The known position of the receiver and the computed position and clock correction for the GPS satellite were used to predict delta range values. First-order ionospheric corrections (2-frequency) and tropospheric corrections (Hopfield model) were also applied. The measured values less the predicted values are termed the raw delta range residuals. These raw residuals were integrated (summed) to produce raw integrated range residuals. After removing a bias and a linear trend, the result is termed integrated range residuals. Figure 5-1 (Ref. 24) plots the integrated range residuals for about a 5 hour segment tracking GPS satellite vehicle 08 on day 64 of 1979 at the Yuma Proving Grounds.

The figure shows that changes of from 1 to 2 cm per minute are common. The only problem with concluding directly from the NSWC data that the signal stabilities involved are compatible with the NOSS goal is in the linear trend that has been removed from the NSWC data. Removing this trend may have removed a significant error source for precision vertical displacement measuring. Given the long duration of the tracking pass and the excellent global stability of the GPS errors, however, it is unlikely that the removed trend is significant when compared to the shorter term effects remaining in the results. The NSWC results are not yet in published form; further investigation may be warranted. At least, the NSWC results show that higher-order drifts (than those linear with time) do not impact the delta range values over even very long tracking periods.

R-62775

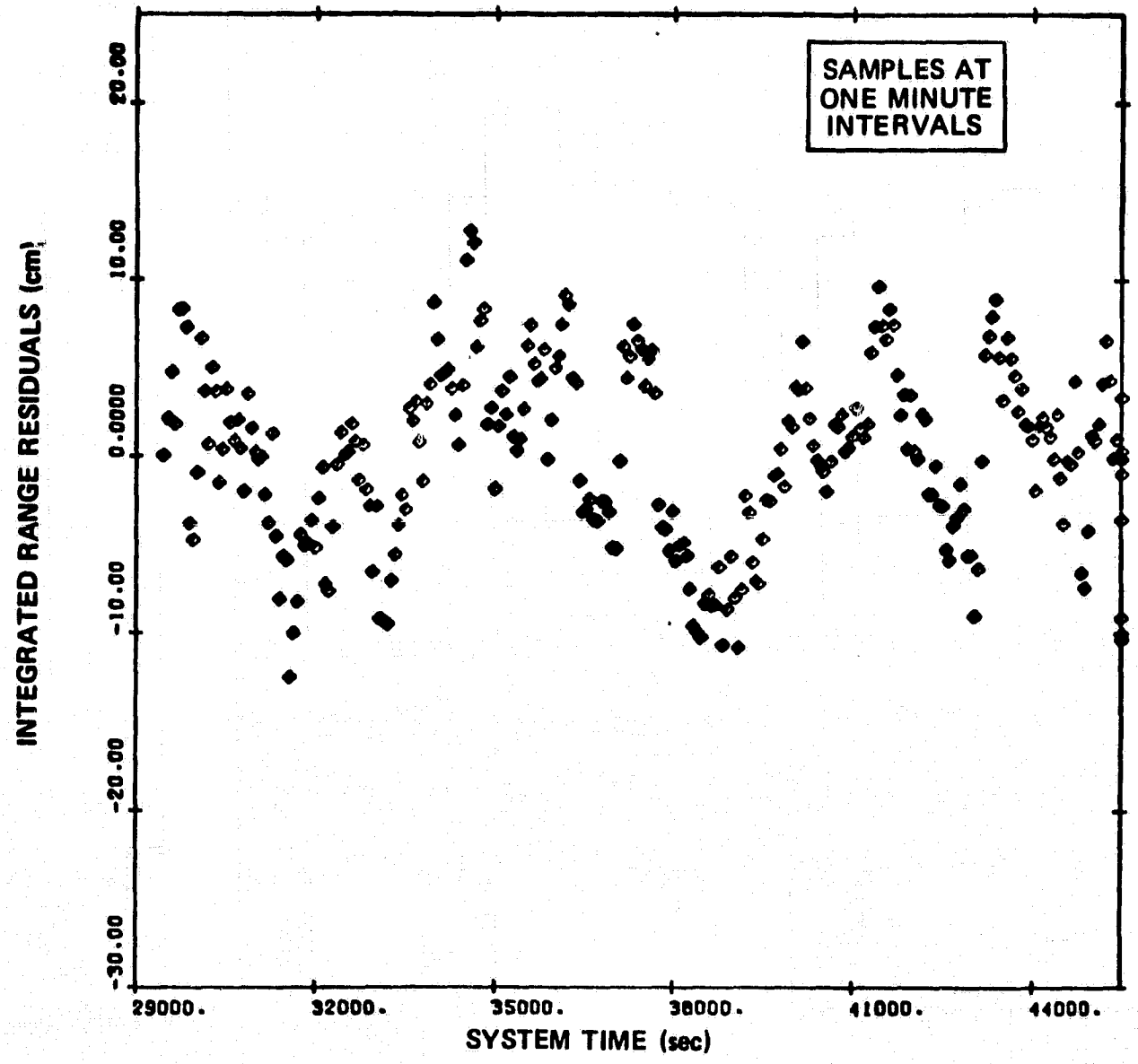

Figure 5-1 Integrated Range Residuals (cm) vs GPS Time (sec), Ref. 24

The preceding discussion suggests that the "first-order" error sources -- receiver measurement error, ionospheric delay, satellite oscillator instability -- may conceivably be

held within tolerable bounds for the vertical displacement measurement. The remainder of this section, however, demonstrates by both intuitive and direct argument that the relative vertical displacement accuracy is sensitive to the absolute position accuracy of either the user vehicle or the GPS satellites (with a sensitivity factor of about 4% in the present case).

Essentially, a measure of relative displacement is a measure of absolute velocity. To measure relative displacement to an accuracy of 5 cm over 67 sec is equivalent to an absolute velocity measurement accuracy of 0.75 mm/sec. Delta range measures the total relative velocity between the user spacecraft and the GPS satellite. Even if these measurements of delta range were perfect, they must be resolved into the proper coordinate frame to be useful. In order to resolve the velocity measurements into the proper coordinate frame, it is necessary to know the position of the user with respect to the positions of the GPS satellites. Errors in this knowledge of position will cause the velocity measures to be misresolved. The error in resolving the velocity measurements will be as large as the total velocity multiplied by the sine of the misresolution angle. This sine is approximately equal to the ratio of the absolute position error divided by the range from the user to the GPS satellite, or

$$\delta v < (v + v_i) \frac{\delta r}{(r - r_i)} \quad . \qquad (5\text{-}1)$$

Using the numerical values

$$\text{NOSS spacecraft} \begin{cases} v = 7505 \text{ mps} \\ r = \text{earth radius} + 700 \text{ km} \end{cases}$$

$$\text{GPS satellite} \quad \begin{cases} v_i = 3875 \text{ mps} \\ r_i = \text{earth radius} + 20183 \text{ km} \end{cases}$$

yields the result that

$$\delta v < (5.84 \times 10^{-4} \text{ 1/sec})\, \delta r. \qquad (5\text{-}2)$$

Comparing this result to the required velocity accuracy shows that an absolute position error of about 1.3 m is tolerable. Another way to put the result is that about 4% of the absolute position error will find its way into the vertical displacement error. This same result may be derived from a more rigorous approach to the problem.

One proposed mechanization for measuring vertical displacement will be termed the "direct approach." The name comes from the fact that this approach uses a deterministic solution for the relative position of the NOSS spacecraft, very much like the determinstic solution for the absolute position given four simultaneous GPS ranging measurements. In this approach, no advantage is taken of the benign spacecraft acceleration environment or of the "smoothing" capability of after-the-fact ground processing. The direct approach is conceptually compatible with real time processing. A description of this approach follows.

A four-channel, P-code GPS receiver is assumed, with each channel coherently carrier tracking an L1 signal from a different satellite. The basic meaurements are four delta ranges, measured as continuous functions of time from some initial time t_o over an interval of duration T. At the initial time, there is assumed available some initial estimate of spacecraft position and clock offset, the source of which is not yet specified. Subsequent to the initial time, the

position of the spacecraft is estimated to be that deterministically consistent with the delta range measurements.

The basic measurements are delta ranges, related to the basic processes by the nominal equations

$$\Delta\rho_i = \left|\vec{r} - \vec{r}_i\right| - \left|\vec{r}_o - \vec{r}_{io}\right| + \phi - \phi_o - \phi_i + \phi_{io} + n_i - n_o \quad , \qquad (5\text{-}3)$$

where

$\Delta\rho_i$ is the measured delta range to the i^{th} GPS satellite, a function of time.

$\vec{r}$ is the NOSS spacecraft position, with $\vec{r}_o$ being the position at the initial time

$\vec{r}_i$ is the i^{th} GPS satellite position, with $\vec{r}_{io}$ being the position at the initial time

ϕ is the receiver clock phase offset from GPS time, with ϕ_o being the offset at the initial time. (Of course, clock phases must be converted to distances by multiplying by the speed of light to be compatible with this discussion.)

ϕ_i is the i^{th} GPS satellite clock phase error after accounting for the satellite clock phase offset by using the navigation data, with ϕ_{io} being the clock error at the initial time

n_i represents all other delta range measurement errors not related to the user or satellite ephemeris and clock condition. This term contains propagation errors and receiver carrier tracking loop errors. n_{io} is the value of these errors at the initial time.

This equation (actually a set of four equations for i=1,2,3,4) is described as being nominal because several small adjustments

are necessary to get nearer the truth, but the adjustments will not affect the ensuing error analysis.* The left hand side of this equation represents what is measured, while the right hand side represents the hidden truth.

Broadcast as part of the navigation message for each of the satellites are some coefficients that, when put into a standard computational process, generate a GPS satellite ephemeris estimate. Of course, this estimate is not free of errors. Assumed available is

$$\vec{r}_{ie} = \vec{r}_i + \delta\vec{r}_i \quad ,$$

$$(\vec{r}_{ieo} = \vec{r}_{io} + \delta\vec{r}_{io}) \quad . \qquad (5\text{-}4)$$

Again, the left hand side of this equation represents a quantity available for computation, while the right hand side represents the truth, serving in this case to define the error in the ephemeris estimate.

No estimate is available for the residual satellite clock phase error ϕ_i or the measurement error n_i, so the best that can be done in constructing an estimate of the NOSS spacecraft ephemeris is to assume that these errors do not exist. Thus, given some initial estimates of the NOSS spacecraft position $\vec{r}_{eo}$ and clock phase offset ϕ_{eo}, the subsequent estimates ($\vec{r}_e$ and ϕ_e) are chosen deterministically to satisfy the equations

$$\Delta\rho_i = \left|\vec{r}_e - \vec{r}_{ie}\right| - \left|\vec{r}_{eo} - \vec{r}_{ieo}\right| + \phi_e - \phi_{eo} \quad . \qquad (5\text{-}5)$$

*Relativistic doppler corrections must be applied, and the positions of the GPS satellites must be referred to the time of signal transmission and not that of signal reception, but, as was remarked, these adjustments needlessly complicate the issue.

With any reasonable NOSS spacecraft-to-GPS satellite geometry, there will be a unique solution to these four, simultaneous, nonlinear equations in four unknowns. This is the direct approach.

The problem now is to analyze the errors in the direct approach. Define the errors in the ephemeris and clock estimates by the relationships

$$\vec{r}_e = \vec{r} + \delta\vec{r} \quad , \tag{5-6}$$

$$\phi_e = \phi + \delta\phi \quad , \tag{5-7}$$

which are also assumed to hold at time zero, with the appropriate subscripts. Now rewrite Eq. 5-5, replacing all estimates by truth and error equivalents

$$\Delta\rho_i = \left|\vec{r} - \vec{r}_i + \delta\vec{r} - \delta\vec{r}_i\right| - \left|\vec{r}_o - \vec{r}_{io} + \delta\vec{r}_o - \delta\vec{r}_{io}\right| + \phi - \phi_o + \delta\phi - \delta\phi_o \quad . \tag{5-8}$$

Expand the vector magnitudes in this equation to first order in the error quantities to obtain the approximate form

$$\Delta\rho_i \approx \left|\vec{r} - \vec{r}_i\right| + \hat{u}_i \cdot (\delta\vec{r} - \delta\vec{r}_i) - \left|\vec{r}_o - \vec{r}_{io}\right| - \hat{u}_{io} \cdot (\delta\vec{r}_o - \delta\vec{r}_{io}) + \phi - \phi_o + \delta\phi - \delta\phi_o \quad , \tag{5-9}$$

where the dots represent vector dot products,

$$\hat{u}_i = \frac{(\vec{r} - \vec{r}_i)}{|\vec{r} - \vec{r}_i|} \qquad (5\text{-}10)$$

is a unit vector from the i^{th} GPS satellite to the NOSS spacecraft, and $\hat{u}_{io}$ is that unit vector at time zero.

Subtract from this approximate result the original truth relationship for the delta ranges (Eq. 5-3) and rearrange terms to obtain the error equation

$$\hat{u}_i \cdot (\delta\vec{r} - \delta\vec{r}_o) + (\delta\phi - \delta\phi_o)$$

$$= \hat{u}_i \cdot (\delta\vec{r}_i - \delta\vec{r}_{io}) + (\hat{u}_i - \hat{u}_{io}) \cdot (\delta\vec{r}_{io} - \delta\vec{r}_o)$$

$$- \phi_i + \phi_{io} + n_i - n_{io} \; . \qquad (5\text{-}11)$$

This equation (regarded as four equations) relates all the various input errors in the process (on the right hand side) to the output errors (on the left hand side) through the measurement geometry implicit in the unit vectors from the satellites to the NOSS spacecraft. These four linear equations in four unknowns may be solved for the output errors in terms of the input errors once the geometry is specified. But these are precisely the same kind of equations that must be solved for the errors in the deterministic solution of vehicle position and clock offset given four ordinary GPS ranging measurements, and the results are well known: the output errors are comparable in size to the input errors, within about a factor of two one way or the other, for reasonably common measurement geometry. So instead of worrying about solving the equations, the sizes of the input error terms on the right hand sides will be evaluated.

The first term on the right hand side of Eq. 5-11 is

$$\hat{u}_i \cdot (\delta\vec{r}_i - \delta\vec{r}_{io}) \quad .$$

In words, this is the component of the relative error in satellite ephemeris along the line from satellite to user. Satellite ephemeris errors are expected to be absolutely accurate to about 1.5 m at all times, and the change in an ephemeris error over a time period of about one min (the period of interest here) will almost surely be much less than 5 cm. In fact, the NSWC data shown earlier is some evidence of this. This input error term will not be the limiting factor in vertical displacement accuracy by the direct method.

The last group of input error terms in Eq. 5-11 is

$$(n_i - n_{io}) - (\phi_i - \phi_{io}) \quad .$$

In words, these terms represent the relative errors in signal propagation, reception, and in satellite clock stability. These errors, too, are included in the NSWC data, with the possibly significant exception of a linear trend. These errors probably may be kept within 2 cm over 1 min.

The remaining term of Eq. 5-11 is

$$(\hat{u}_i - \hat{u}_{io}) \cdot (\delta\vec{r}_{io} - \delta\vec{r}_o) \quad .$$

In words, this term represents the effect of changing measurement geometry on the absolute initial errors in the satellite ephemeris and NOSS spacecraft ephemeris. The first step in evaluating this term is to see how much the geometry can change during the 67 sec tracking interval. By straightforward approximation

$$\hat{u}_i - \hat{u}_{io} \approx \dot{\hat{u}}_i \, \delta t \quad . \tag{5-12}$$

The derivative of the unit vector may be obtained by differentiating the defining Eq. 5-10 and doing a little artful resubstitution:

$$\dot{\hat{u}}_i = \frac{\vec{v} - \vec{v}_i}{|\vec{r} - \vec{r}_i|} - \left[\hat{u}_i \cdot \frac{(\vec{v} - \vec{v}_i)}{|\vec{r} - \vec{r}_i|} \right] \hat{u}_i \quad . \tag{5-13}$$

The largest value for this quantity is obtained when the NOSS spacecraft is directly beneath the GPS satellite and is headed in exactly the opposite direction. Then

$$|\dot{\hat{u}}_i|_{\max} = \frac{v + v_i}{r_i - r} \tag{5-14}$$

Using the same numerical values as in the earlier, heuristic argument, yields a familiar result

$$|\dot{\hat{u}}_i| < 5.84\text{E-}4 \text{ 1/sec.} \tag{5-15}$$

Over a maximum tracking interval of 67 sec, the result is

$$|\hat{u}_i - \hat{u}_{io}| < 0.039 \tag{5-16}$$

Thus, up to 4% (within a factor of two) of the initial absolute error in GPS satellite ephemeris or in NOSS spacecraft ephemeris will find its way into the direct solution for relative NOSS ephemeris over the tracking interval. By implication, an initial absolute error of 1.3 m in either the GPS satellite ephemeris or in the NOSS spacecraft ephemeris will probably just be compatible with the precision relative altitude measurement goal of 5 cm. As has already been remarked

in Chapter 3, the absolute accuracy of the GPS ephemeris is about 1.5 m, so this error alone would produce about 6 cm (from 3 to 12 cm, depending upon the exact geometry) of vertical displacement error.

An absolute estimate of the NOSS spacecraft position based on GPS P-code ranging measurements taken simultaneously with the delta range measurements should be good to about 3 to 5 m per axis -- not good enough to reach the vertical displacement measurement goal. Much of this absolute position error is due to the two-frequency ionospheric delay compensation technique, which tends to amplify receiver code tracking errors. The error in dual frequency ionospheric compensation is largely independent of the size of the ionospheric delays being compensated, so the fact that the NOSS spacecraft is above most of the ionospheric electrons is of no help in reducing the ionospheric compensation errors that dominate the absolute position errors.

On the other hand, the results so far show that vertical displacement may be measured to a precision of 12 to 20 cm over 500 km tracking arcs. The dominant error shows up as a bias in the spacecraft velocity, implying a linear error growth with time in relative displacement estimation. Thus, errors for a 1000 km arc would be from 24 to 40 cm, with values for longer arcs proportionately higher. But the analysis has been quite conservative. Instead of using the so-called "direct approach" to determining vertical displacement, an optimal filtering approach may be used, just as it is for absolute navigation. If the analogy to absolute navigation holds good, the filter approach should reduce errors by a factor of two or more over the direct approach. Further, some worst case errors have been factored into the error analysis for the direct approach; typical errors will be smaller. It is clear that

the precision vertical displacement measurement goal is at the "edge" of GPS capability; more work is necessary to be confident of just which side of the edge the goal is on.

6. CONCLUSIONS AND RECOMMENDATIONS

This report presents the results of a preliminary study of the applicability of NAVSTAR Global Positioning System user equipment to the spacecraft of the National Oceanic Satellite System. The primary focus of the study is on a simple, low cost GPS receiver that could provide semi-autonomous, on board, real time, moderate accuracy navigation and time information for NOSS spacecraft. The secondary focus of the study is on the feasibility of using any configuration of GPS user equipment to provide extreme precision (5 cm) vertical displacement estimation for NOSS spacecraft over tracking arcs of 500 km or more.

There are four major facets to the study of the moderate accuracy GPS receiver for NOSS. One of these is a survey of developmental GPS user equipment most like that suited to NOSS application. Another is a navigation error computer simulation of the receiver in the NOSS environment. The navigation simulation depends, in turn, on the results of a GPS satellite visibility study from NOSS spacecraft orbits and on a summary of navigation error sources pertinent to this moderate accuracy situation.

Major conclusions of the GPS satellite visibility study are:

- By mid 1986, the first launch date projected for NOSS spacecraft, there are expected to be about 12 GPS satellites operational. By the end of 1987 the full constellation of 18 GPS satelites should be in place.

- Orbital details for the operational GPS constellation are not yet firm. Results presented here assume uniform distributions of satellites in three orbital planes. Constellation changes will almost certainly not have any significant impact on moderate accuracy navigation for NOSS spacecraft.

- GPS satellite visibility from a NOSS spacecraft shows no significant variations with the NOSS orbital details over the limited range of orbits considered: circular orbits from 70 to 110 deg inclination, from 600 to 800 km altitude, with arbitrary right ascensions.

- Visibility is a strong function of the GPS receiver antenna coverage and of the number of GPS satellites in the constellation. An antenna pointed at the zenith, covering down to 85 deg from the zenith (almost a hemisphere), will provide fully adequate visibility with 12 satellites or more (See Table 6-1).

TABLE 6-1

VISIBILITY VARIATIONS WITH ZENITH ANGLE LIMIT
(12 SATELLITE CONSTELLATION)

ZENITH ANGLE LIMIT (DEG)	% OF TIME N SATELLITES ARE VISIBLE FOR N EQUALS							AVERAGE NUMBER OF SATELLITES VISIBLE
	2	3	4	5	6	7	8	
80	11	38	40	11				3.52
85	4	25	42	27	2			3.98
90	1	13	36	41	9			4.45
95		4	20	49	26			4.97
100			7	36	57			5.49
105					99	1		6.01
110					55	37	8	6.53

Major conclusions of the navigation error source study are:

- GPS satellite segment errors will not be major sources of navigation error, provided that the receiver is configured to cope with GPS "selective availability" measures for C/A-code operation.
- Signal propagation errors are dominated by ionospheric delay errors for a single frequency receiver. Ionospheric errors are potentially very high (90 m in range measurements) but may be controlled to manageable levels (5 m) by limiting antenna coverage to the 85 deg half-cone about the zenith and by modeling the ionosphere.
- Receiver errors for C/A-code operation are dominated by tracking loop errors that are expected to be about 10 m (1σ) in range and 0.024 mps (1σ) in range-rate.

Major conclusions of the navigation error covariance simulation study are:

- An eight-state extended Kalman filter with some provision for dynamical process noise will be adequate.
- Conservative estimates of rms (1σ) navigation accuracy with single channel, C/A-code tracking and at least 12 GPS satellites operational are 10 m per axis in position and 0.02 mps per axis in velocity (Figs. 6-1 and 6-2).
- Even with the current, very nonuniform, constellation of four GPS satellites (excluding a non-operational satellite and the most recently launched one) rms (1σ) navigation accuracy levels would be 30 m per axis in position and 0.05 mps per axis in velocity, when three satellites were in view, going to 250 m in downrange position and 0.25 mps in radial velocity, after an extended period when no satellites were in view.

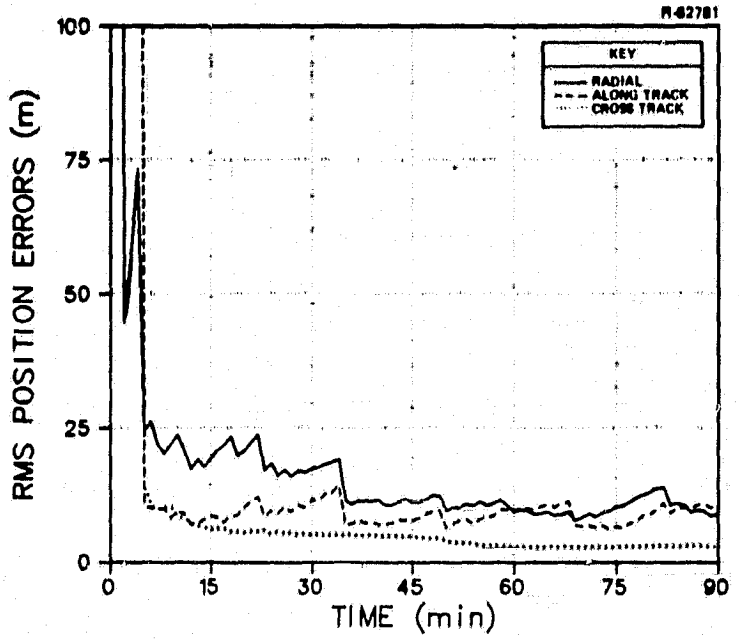

Figure 6-1 RMS Position Error, 12 Satellite Case, Both Pseudo Range and Pseudo Range-Rate Measurements

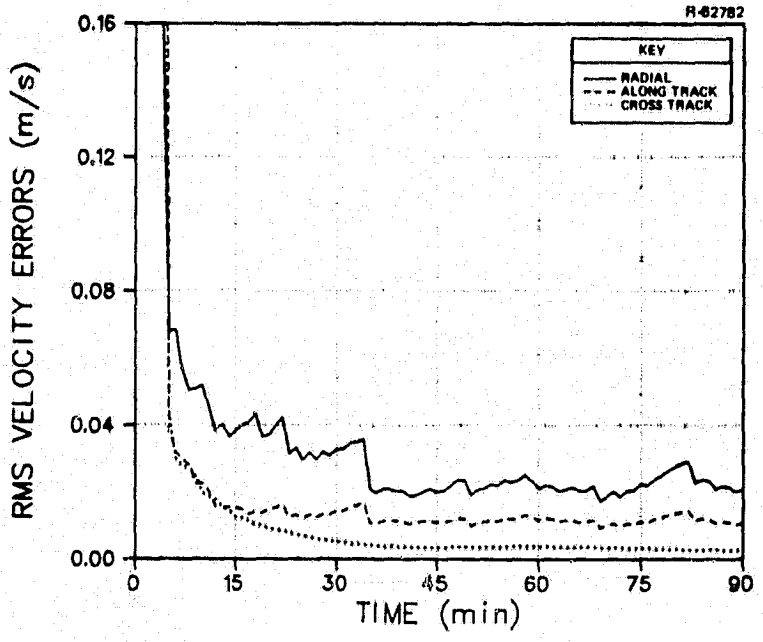

Figure 6-2 RMS Velocity Errors, 12 Satellite Case, Both Pseudo Range and Pseudo Range-Rate Measurements

- Navigation accuracy could probably be improved by especially designing a receiver with low carrier loop noise bandwidths and using long doppler processing times to improve accuracy of range-rate or delta range measurements.

- Using typical receiver design parameters, range-rate or delta range measurements add little to what can be obtained from range measurements alone.

Major conclusions concerning the moderate accuracy GPS user equipment suitable for NOSS spacecraft are:

- A single channel, L1 frequency, C/A-code receiver will be adequate.

- The tracking loops will have to be designed to accommodate the high spacecraft velocities, but this is easy to accomplish.

- A measurement frequency of one to five measurements per minute will be adequate and is easily achievable.

- Such a receiver may be expected to occupy from 4000 to 16000 cc of space, to weigh from 5 to 11 Kg, and to consume from 10 to 25 W of power. The lower values are projections for a 1985 all-digital design, while the higher values are indicative of current development.

- The spacecraft environment and three year mission life will demand very high receiver reliability that will be a major cost driver.

- Provision will be required in the receiver for a command/data link with ground control.

The study of the feasibility of estimating NOSS spacecraft vertical displacement to 5 cm over tracking arcs of 500 km

or more is at a different level than is the study of moderate accurate navigation. This much more demanding goal goes beyond claims for GPS applicability and is approached from a more basic standpoint. The key issues here are measurement types, data processing mechanizations, and fundamental error relationships. Major conclusions of the precision vertical displacement estimation study are:

- It is not clear precisely how to best mechanize the estimation of vertical displacements using GPS measurements; some sort of post-arc optimal filter/smoother working off delta range measurements will probably be best.

- More straightforward mechanizations (the direct approach described in the text) can probably achieve accuracies of 12 to 20 cm over tracking arcs of 500 km. Thus, with a more optimal mechanization, the 5 cm precision vertical displacement measurement goal appears to be near the "edge" of GPS capability.

- The errors in vertical displacement estimates (which are relative position estimates) are dominated by contributions due to absolute position estimation errors. About 4% of the absolute position error will become vertical displacement error in a 500 km tracking arc.

- Based on both theoretical predictions and on experimental results, errors in measuring delta range due to GPS satellite ephemeris and clock errors, due to ionspheric propagation errors, and due to receiver tracking loop errors are probably compatible with the precision vertical displacement accuracy goal.

This study is a preliminary one, laying out the major issues in applying GPS to NOSS and previewing navigation accuracy. Considerable further work will be necessary to actually

specify and develop a moderate accuracy GPS receiver for NOSS, and further work will be necessary to determine if the precision vertical displacement goal is attainable.

One major task that should accompany the development of a GPS receiver for the moderate accuracy navigation application is a direct simulation of the receiver tracking loops interacting with the receiver management software and the navigation filter software. A closed loop simulation of all of these elements is necessary to assure stability and proper action of the navigation filter, especially when "bad" data are encountered. A receiver configured to take advantage of the benign dynamical environment of a NOSS spacecraft will not operate outside of that environment unless the mechanization is altered for test purposes or unless the signal inputs are simulated with a (hardware) GPS signal simulator. Lacking a direct software simulation of the overall receiver operation will make it very difficult to correctly assess tradeoff issues. In fact, it is likely that two such simulations should be maintained: one by the GPS hardware vendor and an independent one by the spacecraft management office to shape and track receiver development and lend confidence to the final product.

The preliminary results on the precision vertical displacement problem are sufficiently enticing that a further, more detailed, study should be made. An optimal filter/smoother mechanization should be developed, and a covariance analysis of this smoother should be simulated. Further analysis of existing GPS doppler data should be done to be confident that the apparent high stability of GPS signals can be realized in the NOSS environment.

APPENDIX A
IONOSPHERIC EFFECTS ON GPS SIGNAL PROPAGATION

The GPS codes that modulate the carrier and are used for ranging measurements travel at the signal group velocity v_g. The travel time from transmission to reception is used to measure the range from transmission to reception and is given by

$$\tau = \int_a^b \frac{ds}{v_g} \quad , \qquad \text{(A-1)}$$

where ds is the differential element of arc length along the signal path from a to b. If it is assumed that the signal travels in a straight line at the speed of light in a vacuum, then the range from a to b is measured as

$$r_m = c\tau \quad . \qquad \text{(A-2)}$$

The error in the measured range due to a group velocity not equal to the speed of light in a vacuum or to bending of the signal path is given by

$$\delta r = \int_a^b \frac{c}{v_g}\, ds - \int_a^b ds \quad , \qquad \text{(A-3)}$$

where the first integral is along the signal path and the second is along the straight line path from a to b.

For the passage of GPS signals through the ionosphere, the errors due to path bending are negligible compared to those

due to signal delay caused by lowered group velocity. Thus, both integrals above may be evaluated along the straight line path from a to b, and

$$\delta r = \int_a^b \left(\frac{c}{v_g} - 1\right) ds \quad . \qquad \text{(A-4)}$$

The ionosphere is a dispersive medium whose index of refraction is a function of signal frequency given (in MKS units) by

$$n(w) = \sqrt{1 - \frac{Ne^2}{m\varepsilon_o w^2}} \quad , \qquad \text{(A-5)}$$

where

N is the density of electrons

e is the charge on an electron

m is the mass of an electron

ε_o is the permittivity of free space.

In a dispersive medium, the group velocity of a modulated wave packet is given by*

$$v_g = \frac{c}{n + w\frac{dn}{dw}} \quad . \qquad \text{(A-6)}$$

For the present case, this group velocity dependence on index of refraction simplifies to

*This result assumes no external magnetic fields present. At GPS frequencies, the effect of the magnetic field of the earth on this result is small.

$$v_g = nc \quad . \tag{A-7}$$

The index of refraction here is only slightly less than unity, so some first order approximations serve to assess the main result:

$$n \quad 1 - \frac{e^2}{2m\varepsilon_o w^2} N \quad , \tag{A-8}$$

$$\delta r \quad \frac{e^2}{2m\varepsilon_o w^2} \int_a^b N \, ds \quad . \tag{A-9}$$

The ionospheric electron density, N, has been left under the integral sign because it varies along the signal path. The other parameters are all constants.

The electron density has both temporal and spatial variations. It depends on local time of day (implying a dependence on longitude), on sunspot activity, on altitude, on latitude, and additionally is subject to rapid fluctuations associated with compression waves travelling through the ionosphere. To consider a worst case situation, the mid latitude, daytime values at a maximum during the eleven-year sunspot cycle may be considered. Figure A-1 (Ref. 25) is an idealized profile of electron density versus altitude for this worst case situation. Figure A-2 replots the same profile on a linear scale for comparison.

To be able to interpret the significance of the electron density profiles, it is necessary to have values for the other parameters involved. In particular

$$e = 1.60206E\text{-}19 \text{ C (Coulomb)}$$

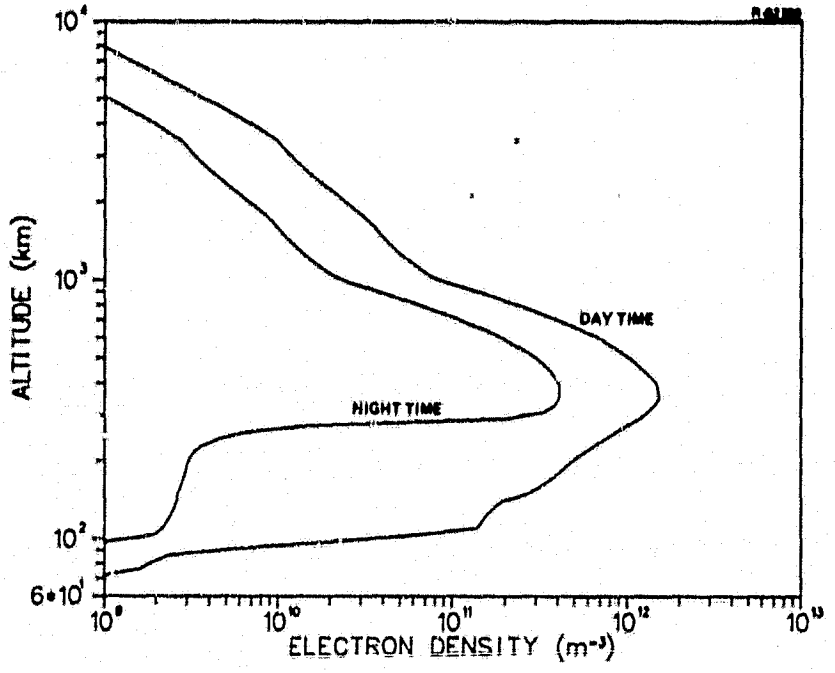

Figure A-1 Idealized Ionospheric Electron Density at a Sunspot Maximum--Logarithmic Scale

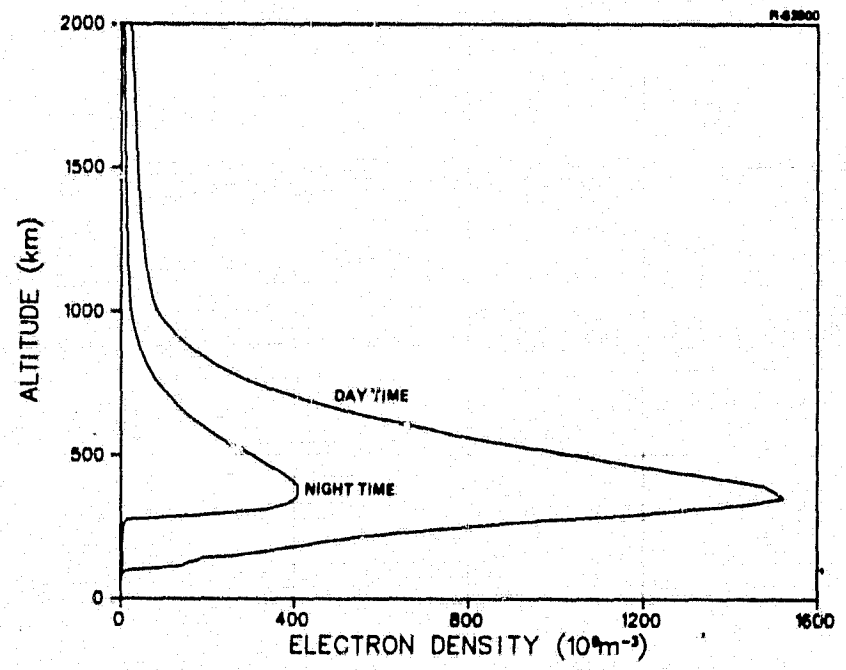

Figure A-2 Idealized Ionospheric Electron Density at a Sunspot Maximum--Linear Scale

$$m = 9.1083E\text{-}31 \text{ kg}$$

$$\varepsilon_o = 8.854E\text{-}12 \text{ f/m (farad/meter)}$$

$$w = 1.57542 \text{ GHz (GPS L1)}.$$

It is also helpful to know that

$$f = C/V \qquad (V = \text{Volt})$$

$$V = J/C \qquad (J = \text{Joule})$$

$$J = \text{kg}\cdot\text{m}^2/\text{sec}^2 \qquad (s = \text{second}).$$

With these values

$$k = \frac{e^2}{2m\varepsilon_o w^2} = 1.62405E\text{-}17 \text{ m}^3 \quad , \qquad \text{(A-10)}$$

and

$$\delta r = k \int_a^b N \, ds \quad . \qquad \text{(A-11)}$$

To get some approximate values for this integral, assume that the electron density depends on altitude alone and postulate the geometric situation illustrated in Fig. A-3. Let s be the distance along the signal path from the user toward the GPS satellite, let h_u be the user altitude, let r_e be the radius of the spherical earth, and let γ be the signal path angle measured from the user zenith. The user radius is just the earth radius plus the user altitude

$$r_u = r_e + h_u \quad , \qquad \text{(A-12)}$$

and the signal altitude is given by

$$h(s) = \sqrt{s^2 + r_u^2 + 2r_u s \cos\gamma} - r_e \quad . \qquad \text{(A-13)}$$

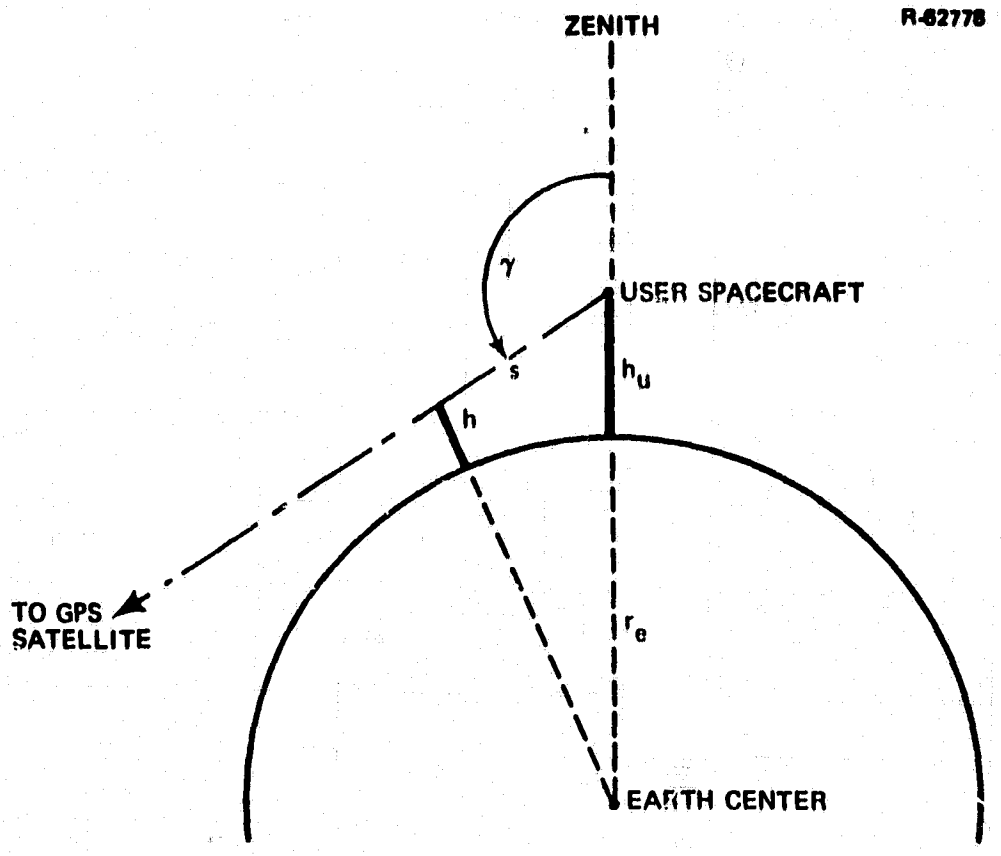

Figure A-3 Signal Path Integration Geometry

The (backwards) signal path terminates at the GPS satellite when the signal altitude equals the given satellite altitude; i.e., when

$$r_e + h = r_s \quad . \tag{A-14}$$

Of course, it is never necessary to carry the integration beyond a few thousand kilometers of signal altitude, as the ionospheric electron density falls to negligible levels at such altitudes.

It is now a reasonably straightforward matter to write a computer program to evaluate the ionospheric delay as

a function of user altitude and signal path zenith angle; i.e., to evaluate

$$\delta r(h_u, \gamma) = k \int_o^{s_m} N[h(s, h_u, \gamma)]\, ds \quad , \qquad \text{(A-15)}$$

where s_m is chosen to correspond to some signal altitude above which negligible contributions to δr occur.

The results of such a computation are presented in Figs. A-4 through A-7, showing the daytime and nighttime values of ionospheric delay at the sunspot maximum over ranges of zenith angle from zero to about the peak values obtainable before the signal path intercepts the earth. The curves have a predictable shape for zenith angles below about 105 deg. In this region, ionospheric delay increases with increasing zenith angle and decreases with increasing user altitude. For each user altitude considered, however, there comes a point where ionospheric delay peaks as a function of zenith angle. This feature of the plots is to be expected from looking at the electron density plot of Fig. A-2. The ionosphere is essentially contained in a spherical shell. Signal paths passing tangentially through this shell suffer the most ionospheric delay. This feature is not evident in ionospheric delay plots for earth-based users, for obvious reasons.

The most striking features of the plots are the large peak delay values, in excess of 90 m at all altitudes under consideration. This plot does represent a worst case situation, and the peak values are achieved at large zenith angles.

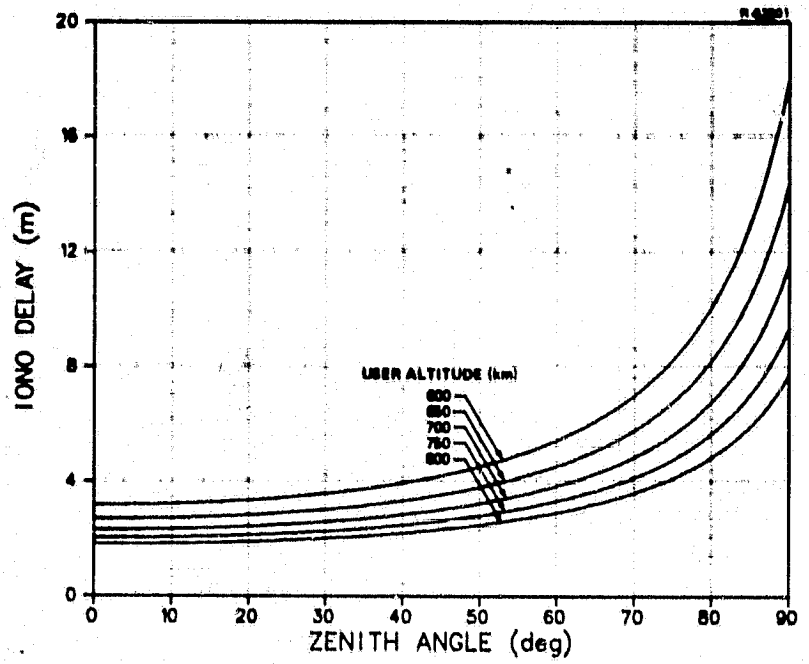

Figure A-4 Daytime Maximum Ionospheric Delay Versus Zenith Angle--0 to 90 deg.

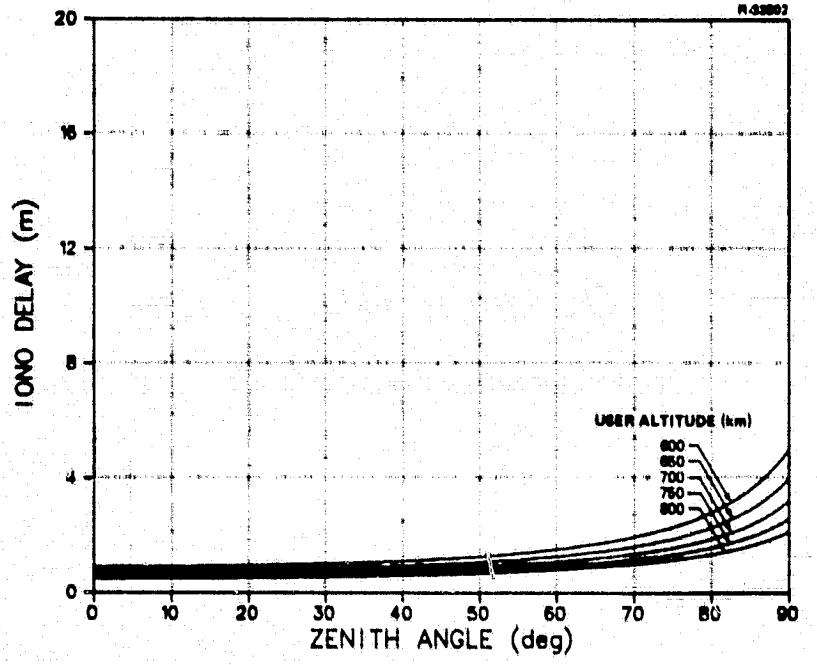

Figure A-5 Nighttime Maximum Ionospheric Delay Versus Zenith Angle--0 to 90 deg.

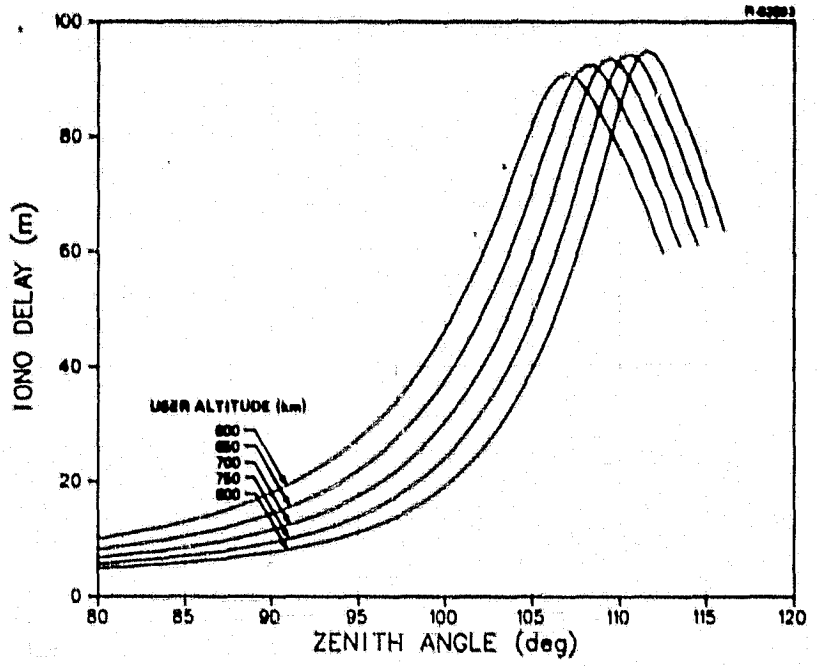

Figure A-6 Daytime Maximum Ionospheric Delay Versus Zenith Angle--80 to 120 deg.

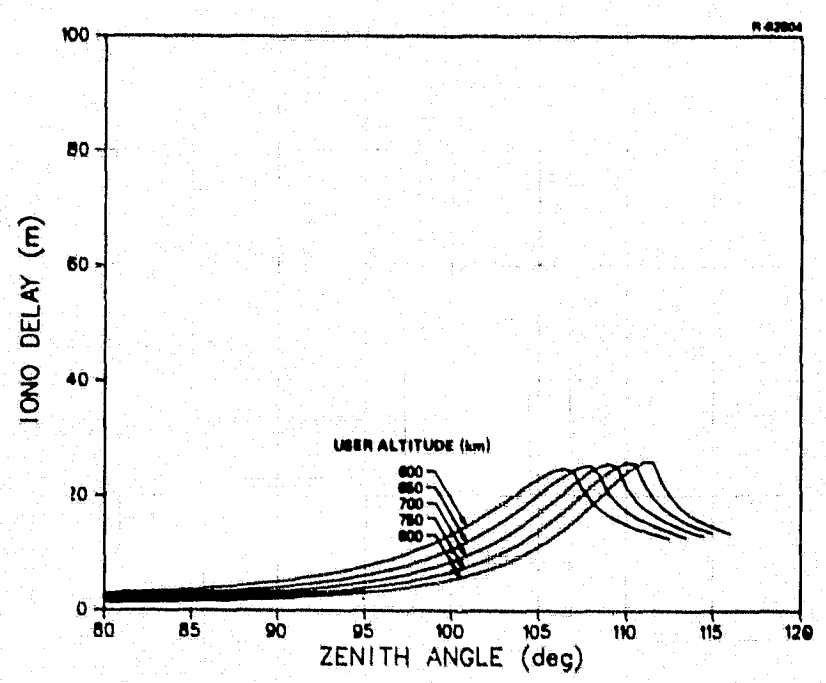

Figure A-7 Nighttime Maximum Ionospheric Delay Versus Zenith Angle--80 to 120 deg.

APPENDIX B
NAVIGATION FILTER SIMULATION DETAILS

The navigation filter used in the covariance simulation has eleven states. They are:

$$\vec{x} = \begin{pmatrix} \vec{r} \\ \vec{v} \\ \mu \\ C_s \\ C_d \\ \phi \\ f \end{pmatrix} \quad \begin{array}{l} \text{vehicle position vector} \\ \text{vehicle velocity vector} \\ \text{gravitational constant} \\ \text{solar radiation pressure constant} \\ \text{air drag acceleration constant} \\ \text{receiver clock phase} \\ \text{receiver clock frequency} \quad . \end{array} \qquad \text{(B-1)}$$

Of course, in the extended Kalman filter whose covariance properties are being simulated, it is only the errors in these states that are actually considered.

The dynamical equations derive from the basic spacecraft dynamics

$$\dot{\vec{r}} = \vec{v} \quad , \qquad \text{(B-2)}$$

$$\dot{\vec{v}} = -\mu \frac{\vec{r}}{r^3} - C_s \varepsilon \frac{\vec{r}_s}{r_s^3} - C_d v \vec{v} \quad , \qquad \text{(B-3)}$$

where

$\vec{r}_s$ is a vector from the vehicle to the sun

ε is 1.0 if the sun is visible to the vehicle, otherwise is 0.0.

In practice, of course, there would be a far more detailed gravitational model used to propagate the position and velocity states, one containing a dozen or more spherical harmonic terms and possibly solar and lunar effects. As long as those terms do not contribute significant errors to the propagation, they may be ignored in the covariance analysis and need not appear in the error dynamical equations developed here.

From the basic dynamics come the linearized error dynamics

$$\dot{\delta\vec{r}} = \delta\vec{v} \quad , \tag{B-4}$$

$$\dot{\delta\vec{v}} = GG(\vec{r})\delta\vec{r} + VV(\vec{v})\delta\vec{v} - \frac{\vec{r}}{r^3}\delta\mu$$

$$-\varepsilon \frac{\vec{r}_s}{r_s^3}\delta C_s - v\vec{v}\,\delta C_d \quad , \tag{B-5}$$

where the gravity gradient matrix is

$$GG(\vec{r}) = \frac{\partial}{\partial \vec{r}^t}\left(-\mu \frac{\vec{r}}{r^3}\right) \quad , \tag{B-6}$$

$$GG(\vec{r}) = \frac{3\mu}{r^5}\begin{pmatrix} r_1^2 - r^2/3 & r_1 r_2 & r_1 r_3 \\ r_1 r_1 & r_2^2 - r^2/3 & r_2 r_3 \\ r_1 r_3 & r_2 r_3 & r_3^2 - r^2/3 \end{pmatrix} , \tag{B-7}$$

and the air drag velocity gradient matrix is

$$VV(\vec{v}) = \frac{\partial}{\partial \vec{v}^t} (-C_d v \vec{v}) \quad , \tag{B-8}$$

$$VV(\vec{v}) = -\frac{C_d}{v} \begin{pmatrix} v_1^2+v^2 & v_1v_2 & v_1v_3 \\ v_1v_2 & v_2^2+v^2 & v_2v_3 \\ v_1v_3 & v_2v_3 & v_3^2+v^2 \end{pmatrix} . \tag{B-9}$$

The positional gradient of the solar radiation pressure is neglected in the linearized error dynamics as being negligible.

The gravitational constant is modeled as just that: a constant

$$\delta\dot{\mu} = 0. \tag{B-10}$$

The solar radiation pressure constant and the air drag acceleration constant are modeled as known constant portions plus unknown portions that are first-order markov processes. That is,

$$C_s = C_{so} + \delta C_s, \tag{B-11}$$

$$\delta\dot{C}_s = -\frac{1}{\tau_s} \delta C_s + \omega_s \quad , \tag{B-12}$$

where τ_s is a time constant for the process, and ω_s is a "white noise" driving term whose intensity is selected to keep the process stationary in the absence of measurements. Similarly, for the air drag acceleration constant

$$C_d = C_{do} + \delta C_d \quad , \tag{B-13}$$

$$\delta\dot{C}_d = -\frac{1}{\tau_d} \delta C_d + \omega_d \quad . \tag{B-14}$$

The stochastic model for the clock errors is simply

$$\delta\dot{\phi} = \delta f + w_{\phi} \quad , \tag{B-15}$$

$$\delta\dot{f} = w_{f} \quad , \tag{B-16}$$

where w_f and w_ϕ are "white noise" driving terms.

In total, then, the state uncertainty satisfies the stochastic differential equation

$$\delta\dot{\vec{x}} = F\,\delta\vec{x} + \vec{w} \quad , \tag{B-17}$$

where, in obvious partitioned form

$$F = \begin{pmatrix} 0 & I & 0 & 0 & 0 & 0 & 0 \\ GG & VV & -\vec{r}/r^3 & -\varepsilon\vec{r}_s/r_s^3 & -v\vec{v} & 0 & 0 \\ 0 & 0 & 0 & 0 & 0 & 0 & 0 \\ 0 & 0 & 0 & -1/\tau_s & 0 & 0 & 0 \\ 0 & 0 & 0 & 0 & -1/\tau_d & 0 & 0 \\ 0 & 0 & 0 & 0 & 0 & 0 & 1 \\ 0 & 0 & 0 & 0 & 0 & 0 & 0 \end{pmatrix} \tag{B-18}$$

The vector white noise intensity matrix is diagonal, with the first seven diagonal elements, corresponding to the position, velocity, and gravitational constant states, all zeros. The final four diagonal elements are denoted as

$$
\begin{aligned}
Q_c(8,8) &= q_s \quad , \\
Q_c(9,9) &= q_d \quad , \\
Q_c(10,10) &= q_\phi \quad , \\
Q_c(11,11) &= q_f \quad .
\end{aligned}
\tag{B-19}
$$

These parameters serve to measure the white noise dynamical inputs.

The covariance of the filter states is denoted by the matrix P, and is the expected value of the self outer product of the uncertainty in the state vector

$$P = E\{\delta\vec{x}\ \delta\vec{x}^T\} \quad . \tag{B-20}$$

Between processing measurements, the covariance propagates according to the differential equation

$$\dot{P} = FP + PF^T + Q_c \quad . \tag{B-21}$$

The measurements processed by the filter are of two types: pseudo range and pseudo range-rate. Pseudo range is defined to be

$$\rho = |\vec{r} - \vec{r}_i| + \phi \quad , \tag{B-22}$$

where $\vec{r}_i$ is the position of the i^{th} GPS satellite (to which the measurement is made). Thus, pseudo range is just the ordinary range from the user to the satellite plus the user clock phase offset with respect to satellite time. Of course, to make this equation dimensionally consistent, the clock phase has to be expressed in units of distance, as is usual when position is more important than time as the navigation output. Simply differentiating the equation for pseudo range gives that for pseudo range-rate as

$$\dot{\rho} = \frac{(\vec{r} - \vec{r}_i)\cdot(\vec{v} - \vec{v}_i)}{\left|\vec{r} - \vec{r}_i\right|} + f \quad . \qquad \text{(B-23)}$$

To simplify these expressions, write

$$\Delta\vec{r} = \vec{r} - \vec{r}_i \quad , \qquad \text{(B-24)}$$

$$\Delta\vec{v} = \vec{v} - \vec{v}_i \quad , \qquad \text{(B-25)}$$

$$\rho = \Delta r + \phi \quad , \qquad \text{(B-26)}$$

$$\dot{\rho} = \frac{\Delta\vec{r}\cdot\Delta\vec{v}}{\Delta r} + f \quad . \qquad \text{(B-27)}$$

The sensitivity of the measurements to the uncertainties of the system state are given by

$$\frac{\partial\rho}{\partial\vec{r}} = \frac{\Delta\vec{r}}{\Delta r} \quad , \qquad \text{(B-28)}$$

$$\frac{\partial\rho}{\partial\phi} = 1 \quad , \qquad \text{(B-29)}$$

$$\frac{\partial\dot{\rho}}{\partial\vec{r}} = \frac{\Delta\vec{v}}{\Delta r} - \frac{\Delta\vec{r}\cdot\Delta\vec{v}}{\Delta r^3}\Delta\vec{r} \quad , \qquad \text{(B-30)}$$

$$\frac{\partial\dot{\rho}}{\partial\vec{v}} = \frac{\Delta\vec{r}}{\Delta r} \quad , \qquad \text{(B-31)}$$

$$\frac{\partial\dot{\rho}}{\partial f} = 1 \quad . \qquad \text{(B-32)}$$

These sensitivities are used to form the linearized measurement matrix, H, expressing either

$$\delta\rho = H_\rho \delta\vec{x} \quad , \tag{B-33}$$

or

$$\delta\dot{\rho} = H_{\dot{\rho}} \delta\vec{x} \quad , \tag{B-34}$$

depending on the type of measurement. In obviously partitioned form

$$H_\rho = \left[\frac{\Delta\vec{r}^T}{\Delta r} \; , \; 0^T, \; 0, \; 0, \; 0, \; 1, \; 0 \right] \quad , \tag{B-35}$$

$$H_{\dot{\rho}} = \left[\frac{\Delta\vec{v}^T}{\Delta r} - \frac{\Delta\vec{r}\cdot\Delta\vec{v}}{\Delta r^3} \Delta\vec{r}^T \; , \; \frac{\Delta\vec{r}^T}{\Delta r} \; , \; 0, \; 0, \; 0, \; 0, \; 1 \right] \quad . \tag{B-36}$$

Associated with each measurement is a measurement noise variance given the general matrix symbol R, although in this case, with scalar measurements, R is also a scalar.

The filter, in processing a measurement, forms the Kalman gain matrix

$$K = P \, H^T [HPH^T + R]^{-1} \quad , \tag{B-37}$$

and multiplies it by the innovation in the measurement (the difference between the measurement and the predicted measurement based on premeasurement state estimates) to form an adjustment to update the estimate of the state of the system. The covariance of the adjusted state is given by

$$P = (I-KH)P \, (I-KH)^T + KRK^T \quad , \tag{B-38}$$

where the P on the right hand side of this "equation" is the pre-update value and that on the left is the improved, post-update value.

If, in fact, the gain used in the above covariance equation were the Kalman gain as shown above, then the covariance update could be accomplished by the simpler, but less numerically stable, equation

$$P = (I-KH)P \quad . \qquad \text{(B-39)}$$

In the filter simulated here, however, the Kalman gain is not used directly. First the three gain states (7, 8, and 9) corresponding to the spacecraft dynamical uncertainties are set to zero, preventing the filter from improving its knowledge of these states and becoming overconfident in its estimates. (The driving noise and time constants for the solar pressure and air drag states can accomplish the same objective for these two states.) Thus, the original, more complex covariance update equation, (Eq. B-38) valid for any gain matrix is used.

Some of the less important numerical details of the simulated filter have also been relegated to this Appendix. They concern the acceleration uncertainty modeling and the user clock modeling.

The gravitational constant uncertainty is set at a very conservative value equivalent to an acceleration uncertainty of 3 μg's. At 700 km of altitude, this works out to a value of

$$\delta\mu = 1.5E+9 \ m^3/sec^2$$

Thus,

$$\sigma_\mu^2 = 2.25E+18 \ m^6/sec^4$$

is used to initialize the (7,7) element of the initial covariance matrix. Since the gain component tending to "calibrate" this uncertainty is set to zero, the uncertainty remains at this value.

The air drag values are computed assuming a 9070 Kg (20000 lbm) spacecraft with an effective area (as viewed from along track) of 67 m^2 (725 ft^2) with a drag coefficient of 2 in an atmosphere of density 3.614E-14 kg/m^3 (for 700 km altitude). This leads to a nominal air drag constant of

$$C_{do} = 2.68E\text{-}16 \ (1/m) \ .$$

(At 700 km altitude, orbital velocity is 7500 m/sec, producing an air drag acceleration of 1.5E-8 m/sec^2 or 1.5E-3 μg.) The uncertainty in this value is assumed to be 20% of the nominal, so

$$\sigma_{C_d}^2 = 2.88E\text{-}33 \ (1/m^2) \ .$$

The time constant associated with this uncertainty (the time for the autocorrelation function to fall to 1/e of the variance) is assumed to be 20 min, less than one-quarter of an orbital period. The intensity of the white noise driving the air drag acceleration uncertainty is selected to keep the process stationary in the absence of measurements. Thus

$$q_d = \frac{2\sigma_d^2}{\tau_d} = 4.8E\text{-}36 \ \ (1/msec^2) \ . \qquad (B\text{-}40)$$

The solar radiation pressure values assume an effective area of the spacecraft (as viewed from the direction that maximizes area) of 88 m^2 (950 ft^2). Solar radiation pressure is 4.56E-6 N/m^2 (9.53E-8 lb/ft^2). This results in a nominal

acceleration due to solar pressure of 4.4E-8 m/s^2 or 4.5E-3 μg. Assuming that 20% of this nominal value is an uncertainty and that the distance to the sun is about one astronomical unit of 1.5E+11 m, leads to the values

$$\delta C_s = 2.0E+14 \ (m^3/sec^2) \quad ,$$

$$\sigma_s^2 = 4.0E+28 \ (m^6/sec^4) \quad .$$

Again, a time constant of 20 min is used, and the driving noise intensity is selected for stationarity

$$q_s = \frac{2\sigma_s^2}{\tau_s} = 6.7E+25 \ (m^6/sec^5) \quad . \qquad \text{(B-41)}$$

Gravitational constant uncertainty produces acceleration uncertainty in the radial direction only, and air drag uncertainty produces acceleration uncertainty in the along track direction only. Thus, for purposes of simulation, the sun was placed normal to the orbit plane so that solar pressure uncertainty would produce only cross track acceleration uncertainty. This assumption may not be compatible with the assumed maximal solar area of the spacecraft, but the assumption is a conservative one. Also, the sun does not rise or set when it is normal to the orbit plane, so solar pressure is always operative in the simulation.

If the clock were initialized with no errors in phase or frequency, the rms phase error after a time T, due to the driving white noises, would be

$$\sigma_\phi = \sqrt{q_\phi T + q_f T^3/3} \quad . \qquad \text{(B-42)}$$

The noise intensity values are selected to model a medium quality quartz crystal oscillator with fractional frequency stability of 3.3 parts in 10^{10} (or about 0.1 mps when multiplied by the speed of light) over time periods from 1 min to 20 min. These time values are used because they are characteristic of the time spans over which the navigation filter must "connect" measurements depending on the clock. The values

$$q_\phi = 5.7E\text{-}1 \ (m^2/sec) \quad ,$$

$$q_f = 2.4E\text{-}5 \ (m^2/sec^3) \quad ,$$

produce the equivalent fractional frequency stability values given in Table B-1.

TABLE B-1
CLOCK MODEL FRACTIONAL FREQUENCY STABILITY

PERIOD (min)	FRACTIONAL FREQUENCY STABILITY	
	ABSOLUTE	mps
0.1	1.0E-9	0.30
1	3.3E-10	0.10
5	2.2E-10	0.07
20	3.3E-10	0.10
60	5.7E-10	0.17

REFERENCES

1. "Space Vehicle Nav. Subsystem & NTS PRN Navigation Assembly/User System Segment & Monitor Station," Rockwell International Corporation, Space Division, Document Number MH08-00002-400, Rev. G., August 1979.

2. "Draft System Specification for the NAVSTAR Global Positioning System, Phase II," SAMSO/YEN, SS-GPS-200, September 1977.

3. Milliken, R.J., and Zoller, C.J., "Principle of Operation of NAVSTAR and System Characteristics," Navigation, Vol. 25, No. 2, Summer 1978.

4. Spilker, J.J.,Jr., "GPS Signal Structure and Performance Characteristics," Navigation, Vol. 25, No. 2, Summer 1978.

5. Van Dierendonck, A.J., et al., "The GPS Navigation Message," Navigation, Vol. 25, No. 2, Summer 1978.

6. Glazer, B.G., "GPS Receiver Operation," Navigation, Vol. 25, No. 2, Summer 1978.

7. Borel, M.J., et al., "Texas Instrument Phase I GPS User Equipment," Navigation, Vol. 25, No. 2, Summer 1978.

8. Martin, E.H., "GPS User Equipment Error Models," Navigation, Vol. 25, No. 2, Summer 1978.

9. "Draft System Segment Specification for the User System Segment, NAVSTAR Global Positioning System, Phase II," SAMSO/YEN, SS-US-200, September 1977.

10. Moses, J., and Martin, E., "GPS Missile Receiver Study and Costing Analysis," Magnavox Advanced Products Division, MRL Reference No. R-5559, February 1977.

11. "Preliminary Design Review of the Receiver/Processor Assembly (R/PA)," Magnavox Government and Industrial Electronics Company, March 1977.

12. Duiven, E.M., and Connolly, P.E., "GPS Satellite-to-Satellite Tracking Study Results," The Analytic Sciences Corporation, Technical Report TR-1041, January 1978.

REFERENCES (Continued)

13. Pyle, R.H., and Rains, R.G., "Global Positioning System (Phase I) Error Analysis," The Analytic Sciences Corporation, Technical Report TR-428-1, August 1974.

14. Duiven, E.M., and LeSchack, A.R., "Global Positioning System Simulation Development and Analysis," The Analytic Sciences Corporation, Technical Report TR-428-2, December 1974.

15. Farr, J. E., "Space Navigation Using the NAVSTAR Global Positioning System (GPS)," Guidance and Control 1979, Volume 39, Advances in the Astronautical Sciences, American Astronautical Society.

16. Matchett, G.A. et. al., "Space Shuttle Navigation Analysis Final Report, Volume I - GPS Aided Navigation," The Analytic Sciences Corporation, Technical Report TR-1001-1-1, May 1980.

17. Macdonald, T.J., and Jones, H.L., "Tactical GPS Guidance Evaluation (U)," The Analytic Sciences Corporation, Technical Report TR-978-1, July 1979. (CONFIDENTIAL)

18. Brammer, R.F., Himes, J.G., and Shields, J.D., "Evaluation of GPS Tactical Missile Guidance," The Analytic Sciences Corporation, Technical Report TR-625-2, December 1975.

19. Brammer, R.F., and Himes, J.G., "Evaluation of Jamming Resistant GPS Receivers with Application to Tactical Missile Guidance," The Analytic Sciences Corporation, Technical Report TR-625-3, August 1976.

20. Macdonald, T.J., Jones, H.L., and Vogel, M.A., "GPS High Anti-Jam Performance Analysis," The Analytic Sciences Corporation, Technical Report AFAL-TR-79-1038, June 1979.

21. Macdonald, T.J., and Vogel, M.A., "GPS-Aided Navigation Analysis," The Analytic Sciences Corporation, Technical Report TR-1560-1, April 1980.

22. Macdonald, T.J., "Tactical GPS Adaptive Bandwidth Study," The Analytic Sciences Corporation, Technical Report TR-1261-1, January 1980. (CONFIDENTIAL)

REFERENCES (Continued)

23. Hill, R., and Hermann, B.R., "Preliminary Results from the Doppler Van," Naval Surface Weapons Center, Dahlgren, Va., unpublished notes.

24. Hermann, B.R., "NGRS Correlated Range Residuals," Naval Surface Weapons Center, Dahlgren, Va., private communication.

25. Evans, J.V., and Hagfors, T. Radar Astronomy, McGraw-Hill, 1968.